UNIVERSIDADE D
COIMBRA

André Eduardo Rosado Cupido dos Santos

PERFORMANCE ASSESSMENT OF PHOTONIC SUPPORTED BEAM STEERING TECHNIQUES

Dissertação no âmbito do Mestrado Integrado em Engenharia Eletrotécnica e de Computadores, área de Especialização em Telecomunicações orientada pela Professora Doutora Maria do Carmo Raposo de Medeiros e apresentada no Departamento de Engenharia Eletrotécnica da Universidade de Coimbra.

September de 2019

Performance Assessment of Photonic Supported Beam Steering Techniques

Dissertação no âmbito do Mestrado Integrado em Engenharia Eletrotécnica e de Computadores, área de Especialização em Telecomunicações orientada pela Professora Doutora Maria do Carmo Raposo de Medeiros e apresentada no Departamento de Engenharia Eletrotécnica da Universidade de Coimbra.

Examination Comitee

President: Prof. Luís Alberto da Silva Cruz

Member: Prof. Tiago André Nogueira Morgado

Supervisor: Prof. Maria do Carmo Raposo de Medeiros

The work developed in this dissertation was carried out within the framework of the projects Project UID/EEA/50008, sub-project PhoTech-5G/60GH, RETIOT, SAICT-45-2015-03 Project nº 16432, and supported by the IT infrastructure facilities namely the ORCIP Centro-01-0145-FEDER-002141.

Acknowledgements

I would like to say a special thanks to my supervisor Prof. Maria do Carmo Raposo de Medeiros for helping me in my masters degree, without her this would not be possible. Also, a special thanks to my girlfriend for being there for me. And to all my friends and family.

For all of you thank you.

Resumo

O tema desta dissertação é a implementação de um modelo de simulação para a avaliação de técnicas fotónicas de direcionamento de feixe de ondas milimétricas, no contexto da rede de 5ª geração (5G). A grande largura de banda disponível na gama de frequências é essencial para suportar o crescente aumento de serviços que necessitam de grande largura de banda, nomeadamente, serviços interativos e multimédia.

Contudo, a transmissão atmosférica na região das ondas milimétricas é caraterizada por uma elevada atenuação, que pode ser combatida através da utilização de feixes hertzianos estreitos e direcionais. A direccionalidade do feixe implica que para se cobrir uma determinada área geográfica é conveniente que a direção do feixe consiga ser controlada, e alterada dinamicamente de acordo com as necessidades de comunicação dos utilizados. De acordo com a teoria dos agregados de antenas isto é possível manipulando o atraso relativo dos sinais que alimentam os vários elementos do agregado. Como é difícil implementar linhas de atraso ideais em rádio frequência o que é normalmente utilizado é a aplicação de um desvio de fase relativo ao sinal que alimenta os vários elementos do agregado. No entanto, esta estratégia causa deformação do feixe. Recentemente, várias técnicas fotónicas têm sido propostas e demonstrado serem capazes de permitirem impor atrasos a sinais de alta frequência. No entanto, para além da demonstração do potencial das várias técnicas é necessário estudar o seu efeito no desempenho de sistema de comunicação. É este o tema do trabalho desenvolvido nesta dissertação.

Mesmo as técnicas fotónicas quando implementadas não são ideais e causam deformação do feixe. Nesta dissertação para além de se quantificar o efeito da deformação do feixe que é introduzida através do uso de um interferómetro de Mach-Zehnder também é demonstrado que os efeitos da deformação do feixe podem ser parcialmente compensados digitalmente através de um equalizador de canal.

Palavras Chave

Antenas; Beam Forming; Beam Steering; Mach-Zehnder interferometer; Ondas Milimetricas; Phased array antenna; Fotonica; Optical true time delay; Tunable True Time Delay

Abstract

The topic of this dissertation is the implementation of a simulation model to assess the performance of photonic supported techniques for beam steering in the context of 5G. The operation in the Millimetre wave (mmWave) band is currently an important research topic in the communication domain motivated mainly by the amount of available bandwidth that will enable the very high bit rates sought for 5G and beyond 5G communication systems.

The blockage effect, propagation loss and high directionality that needs beam alignment are the main challenges for mmWave communication links. To cover a larger area efficiently, the antennas will need to have beam steering and beam forming capabilities. Phased array antennas (PAA) that consists of an array of multiple antenna elements (AEs), enable beam steering that relies on microwave phase shifters which are used to control the phase of each AE. Microwave electrical phase shifters suffer from beam-squint problem which limits the operation bandwidth. Beam quint leads to different frequencies being steered in different directions. This problem can be solved by using true time delay lines (TTDL) which ensures a frequency-independent steering angle. However, TTDL with large bandwidth are difficult to implement in the electronic domain. Conversely, microwave photonics (MWP) where the signal processing is done relying on photonic offers large bandwidth.

In this dissertation a simulation platform able to assess the effect of the Beam Squint on the performance of a wireless system was developed in Matlab®. The simulation platform is used to assess performance degradation due to the Beam Squint of extra-high bandwidth mm-wave links that employ Orthogonal Frequency Division Multiplexing (OFDM) signals. We assess the performance of an optical tunable true time delay based on a Mach-Zehnder Interferometer (MZI) to replace the electrical phase shifters and decrease the Squint Effect. The simulation platform developed in Matlab® is prepared to test other methods of beam squint compensation for future use. We also explored the possibility of digitally compensating the Squint Effect in the receiver.

Keywords

Antennas; Beam Forming; Beam Steering; Mach-Zehnder interferometer; Millimetre Waves; Phased array antenna; Photonics; Optical true time delay; Tunable True Time Delay.

Table of Contents

List of Figures

List of Tables

List of Acronyms

ADC	Analog to Digital Converter
AEs	Antenna Elements
AWG	Arrayed waveguide grating feedback
BER	Bit Error Rate
CPRI	Common Public Radio Interface
CT-MZI	Continuously Tunable Mach-Zehnder Interferometer
DAC	Digital to Analog Converter
EOM	Electric-Optic Modulator
EVM	Error Vector Magnitude
FSR	Free Spectral Range
IIR	infinite impulse response
MMB	Millimetre-wave mobile Broadband
mmWave	Millimetre Wave
MWP	Microwave Photonics
MZ	Mach-Zehnder
OFDM	Orthogonal Frequency Division Multiplexing
PAA	Phased Array Antenna
PA	Phased Array
PICs	Photonic Integrated Circuits
QAM	Quadrature Amplitude Modelling
QoS	Quality of Service
RF	Radio Frequency
TTR	True-time-delay

1 Introduction

1.1 Motivation

Nowadays practically everyone has a mobile device and those numbers are getting higher, parallelly, the number of interactive multimedia applications is also increasing and this trend will continue in the future [1]. Video-based applications generate a huge amount of wireless traffic that needs to be transmitted at high speed. The increasing video quality and number of connected devices with access to those video entertainment services will cause an immense increase in traffic that soon, will not be supported by the current generation wireless network. To cope with all this, the next generation wireless network needs to have higher bandwidth, and to achieve this, the wireless network frequency has to move out of the current overloaded frequency spectrum [2] and occupy higher frequencies bands in the mmWave region [3].

The mmWave region is defined as the spectral region between 30 and 300 GHz, this translates in a wavelength of 10mm and 1mm respectively, thus the mmWave designation. Although today we are still not certain of which mmWave bands will be used by fifth generation (5G) technologies, there are several proposals and tests being made to select the most appropriated. One of which is the 28 GHz band used for Outdoor Backhaul for Fixed Wireless Access and Moving Hotspots [3], this band was tested in the winter Olympic games of 2018 delivering real-time 4k video of the event. Although the band is used for satellite communications, this band is promising for future 5G applications, in [4] it was demonstrated that it can support cellular communications in the range of 500 meters. Another possible band is the unlicensed 60 GHz band, currently used by IEEE802.11ad/WiGig [5], this one is expected to be tested at the Tokyo-Narita airport during the Tokyo Summer Olympics games in 2020. These bands offer relatively wide available spectrum. The mmWave band offers wide available spectrum and the size of the antennas and mmWave circuits can be decreased significantly compared to third generation (3G) and fourth generation (4G) systems.

Despite the potential of mmWave wireless systems, there are a number of key challenges that need to be overcome [6]. In this dissertation, we focus on the constraints related with the propagation loss. According to Friis transmission equation [7], given by equation (1.1), the transmission loss is directly proportional to the square of the radio signal frequency. i.e, the ratio between received power (P_r) and transmitted power (P_t) is inversely proportional to the square of the frequency, *f*, meaning higher frequencies suffer higher losses.

$$\frac{P_r}{P_t} = \frac{A_1(\theta_1, \phi_1) A_2(\theta_2, \phi_2)}{(\lambda r)^2} \tag{1.1}$$

Where r is the distance between antennas, $A_1(\theta_1, \phi_1)$ and $A_2(\theta_2, \phi_2)$ are respectively the transmitting (1) and receiving antenna (2) apertures. $\theta_i, \phi_i, i = 1,2$ are elevation and azimuth angles. λ is wavelength of the signal (λ=c/f), where c is the speed of light.

1.2 Beam Forming and Beam Steering

To address the problem of high transmission loss the next generation network will need high gain and directional antennas and consequently more points of access, meaning a new architecture for the network [8]. To cover a large area efficiently, the access points will need to have beam steering and beam forming capabilities [9]. Beamforming and beam steering are timely topics that are intensively studied [10]. Beamforming is a term that refers to the formation of a beam of energy from a specific set of antenna elements (AEs) (PAA), a *phased array antenna*, while beam steering is the variation of direction of the main lobe of the antenna radiation pattern.

1.3 Phased Array Antenna

A transmitter PAA, as illustrated in Figure 1. 1, consists of an aggregate of *N* antennas elements, the relative phases of the signals feeding the AEs are set in such a way that the effective radiation pattern of the array is intensified in a desired direction and suppressed in undesired directions. The total radiated field of an array is a vector superposition of the fields radiated by the individual elements. The resulting total radiated electric field is the vector sum of all electric fields from each antenna elements, forming a directional and high gain beam. The PAA radiation pattern can be controlled by geometrical configuration of array, relative placement of antenna elements, excitation pattern of the individual elements and the individual pattern of each antenna element [7], [11], [12].

In this dissertation, the case of equally spaced antenna elements is considered, being *d* the distance between consecutive antenna elements.

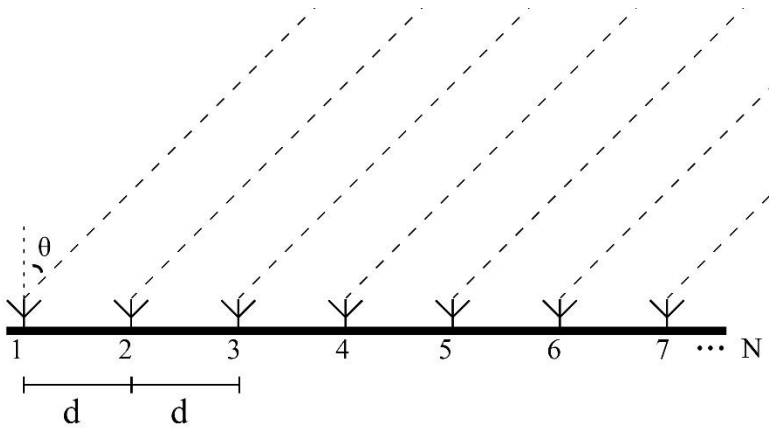

Figure 1. 1 - Example of an N element linear array

In mmWave wireless system there are two types of antennas that are widely used, horn antennas and microstrip. Although horn antennas have a higher gain and directivity, in this dissertation we focus on microstrip antennas because of its favourable characteristics, they are not very expensive compared with horn antennas, easy to fabricate and, being just a small patch, they can easily form a large array. They also have a very extensive and varied set of applications, for example systems with high aerodynamic needs like airplanes or cars.

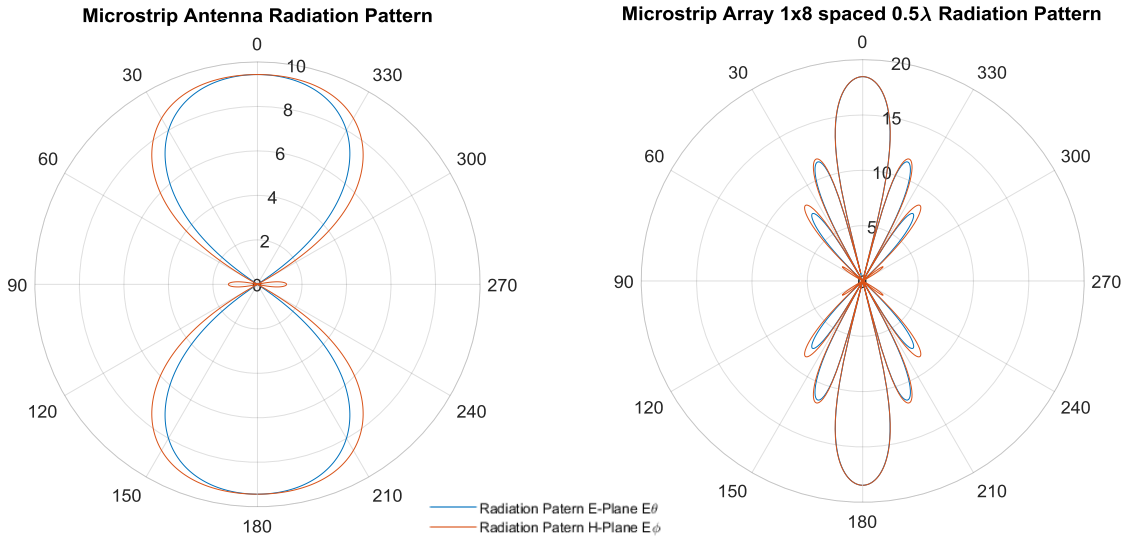

Figure 1. 2 -Polar radiation pattern of individual antennas element (left), polar radiation pattern of an array 1x8 (right)

By controlling the progressive phase shift of the antennas elements we can control the direction in which the electric fields add up constructively. Figure 1. 2 shows an illustrative example of a far field radiation pattern of an individual microstrip antenna element (left) and the far field radiation pattern of a linear array of eight microstrip antennas equally spaced elements (right). The radiation patterns are represented in a polar diagram format and indicate the field intensity in dB with the angles in degrees.

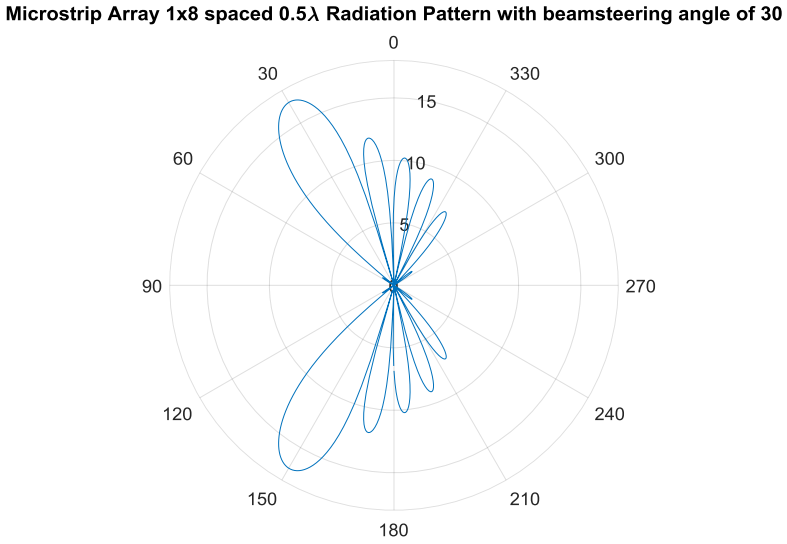

Figure 1. 3 - Example of beam steering to 30º

From Figure 1. 2 it is clear, as it was expected, that using antenna arrays we can improve the gain and the directivity of the radiation pattern, that allows for a better compensation of path loss associated with the high frequency. However, to cover a wide area efficiently we need to steer the beam, which can be achieved by controlling the relative phases of the signals that feed the antenna elements. Figure 1. 3 shows a radiation pattern of a beam directed towards a 30º degree, the sum of the signals of all the array's elements add themselves constructively in the 30º direction, the gain reduces roughly 2dBs but it is still well above the gain of a single antenna element.

1.4 Problem Identification: The Beam Squint Problem

The steering operation of traditional PAAs relies on microwave phase shifters which are used to control the phase of each antenna element. Beam squint arises due to the dependence of beam steering angle on the microwave frequency which leads to the divergence of beam directions of different microwave. If a phase shifter is designed to direct the beam of a 60 GHz signal towards 30º, if the PAA is fed with signal of 61 GHz, it will direct it towards another direction as illustrated in Figure 1. 4. This effect is particularly noticeable when high bandwidth signals are transmitted. The beam squint phenomenon is the broadening of the beam that is observed when using a regular phase shift in a high bandwidth system, as we can see in the area covered will be compromised for high bandwidth systems, this will introduce losses and reduce the QoS.

For example, a signal with 10 GHz bandwidth, centered at 60 GHz. Considering only the field intensity, if the phase shift is designed to direct the beam to 30º at 60 GHz, the signal frequency components at 55 GHz and 65 GHz, will be directed towards other directions. A receiving antenna located at 30º will receive the signal power components at 55 GHz and 65 GHz attenuated relatively to the 60 GHz components, therefore the signal will be distorted.

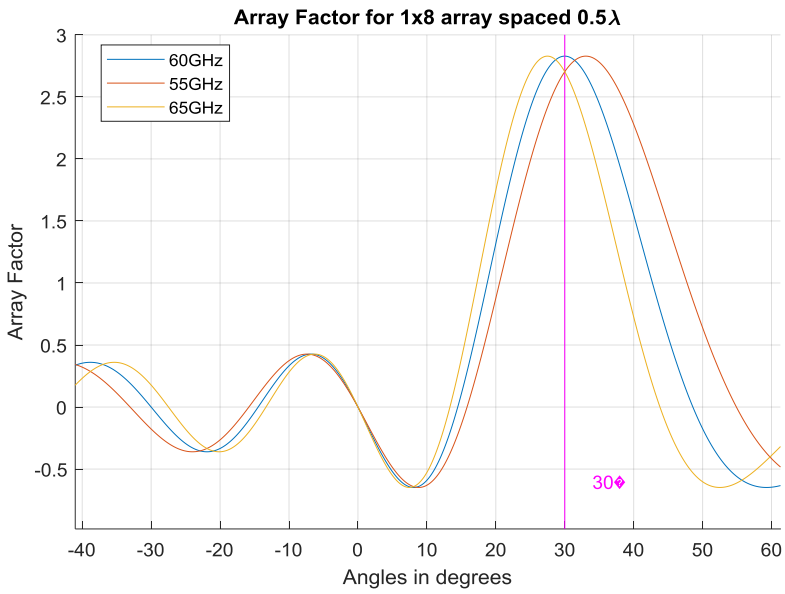

Figure 1. 4 - Array Factor dependency with frequency

The desired direction is not always covered with maximum power by all signal's frequency components, in this condition, the desired quality of service may not be achieved. Another down side of the phase shifts is the difficult implementation of a tuneable phase shift and the losses associated [13].

Digital signal processing is a research line that is under consideration, however, the network will be more complex and less power efficient because of all the analogue-to-digital converters (ADC), digital-to-analogue converters (DAC)[10] and processing units needed for each antennas element of the array.

Other approaches to avoid beam squint relying on true-time delays (TTDs) have been pursued. TTDs provide phase shifts that vary linearly with the operating frequency enabling frequency independent steering angles, and consequently, avoiding beam squint. However, reported electronic implementation of TTDs have high loss, limited bandwidth and to not allow for fast steering tuneability.

Recently photonic delay line as well as photonic phase shifters have emerged as promising candidates for beam steering[14]–[18]. In fact, several implementations and demonstrations of photonic integrated circuits (PICs) aimed to beam steering have been reported recently [19][20]. In photonic supported beam steering, the mmWave signal received by the antenna element modulates an optical carrier and therefore it is translated to the optical domain, the optical signal is then optically delayed, or phase modulated to acquire the required delay. After, the resultant optical signal is photodetected and a delayed version of the mmWave signal is obtained. The published work in the field, is mainly focused on the design, fabrication and characterization of the devices, however the effect of the devices on the performance of the communication system is still missing. This is the objective of this dissertation.

1.5 Work Objectives and Methodology

The final objective of this dissertation is to implement a simulation platform, in Matlab®, to evaluate the performance of photonic supported beam steering techniques at the system level.

To achieve the final objective the following intermediate objectives are identified:

- Objective 1 – Implementation of a Radio Frequency (RF) system model, firstly using a general two-dimension formulation with a linear array.
- Objective 2 - Add to the software model electric phase shift elements that do not provide true time delay, the objective is to introduce controlled beam squint.
- Objective 3 - Identify the figures of merit that quantify the squint effect.
- Objective 4 - Include a photonic supported phase shifter in the simulation platform. The phase shifter that will be considered is made by a non-resonant optical delay line based on a tuneable MZ interferometer [21].
- Objective 5 - Evaluation of the performance of the photonic supported phase shifter.
- Objective 6 - Optimize the design of the photonic supported phase shifter.
- Objective 7– Study the performance of typical 5G system when beam steering is employed.

1.6 Contributions

In this dissertation we identify the following contributions:

- Development of a Matlab program to simulate the radiation pattern of horn and microstrip antennas;
    - Include the capability to simulate phased arrays with beam steering functionality;
- Development of a Matlab program to visualize the squint phenomenon;
- Development of a Matlab program to visualize and design the transfer function of the optical true time delay system to match the specifications needed;
- Development of a Matlab program to create an Orthogonal Frequency Division Multiplexed (OFDM) signal and simulate its transmission measuring and comparing various system performance;
    - System without beam steering capabilities;
    - System with Phase Shift;

- System with ideal true time delay;
- System with optical true time delay.

The last Matlab program was designed to test different methods in the future.

1.7 Dissertation Structure

This dissertation is organized in six chapters. In the first chapter entitled “Introduction” we discuss the context and motivation for this work, introduce phased arrays and beamforming, identify the problem, objectives and methodology and enumerate the contributions made. In the second chapter, we discuss some networks architectures and applications. In chapter 3 the basic principles of beam forming and beam steering are presented. Following this, the dissertation focuses on the beam forming technique based on electric phase shifters. Next, beam squint is explained and identified as the principal limitation of beam forming techniques based on electric phase shifters and the figures of merit used to evaluate the quality of the beam steering are presented. At last, an overview of the different techniques employed for beam forming and beam steering are identified. In chapter 4 the simulation system model with the electric phase shifter is explained and its performance is evaluated varying different parameters of the signal and system to see how it affects the squint effect. Digital beam squint compensation is explained and applied, its limitations are exploited. In chapter 5, Photonic based mmWave time delays are then identified as a solution to overcome the squint problem. To ensure beam steering capability we need not only to have a true time delay, but also a tuneable true time delay. In this work we are going to focus on the implementation of a tuneable true time delay based on a Mach-Zehnder (MZ) interferometer equipped with two tuneable couplers. the device is going to be integrated in a system. The system simulation model is explained and it is used to assess the system performance. The dissertation final chapter is dedicated to the conclusions and future work.

2 mmWave Architectures and Application Scenarios

2.1 Introduction

In this chapter we discuss possible future mobile network architectures and application scenarios that require ultra-high data transmission speed and low transmission latency.

2.2 5G Network Architecture

One possible network architecture for 5G outdoor mobile technologies is mmWave mobile broadband (MMB) presented in [3] and [8], it uses the current generation network's 4G base stations and adds the necessary MMB base stations to assure quality of service in areas of interest, reducing the investment needed in the 5G infrastructure.

The architecture in Figure 2. 1 uses an optical distribution of the mmWave signals between base stations, therefore it is suitable to apply a phase shift in the optical domain. Hence, when we compare this architecture with one that implements the phase shift in the electrical domain, we can predict that the one with the optical phase shifter is going to be more energy-efficient, is going to have less complexity and it will assure the requirements for 5G technologies.

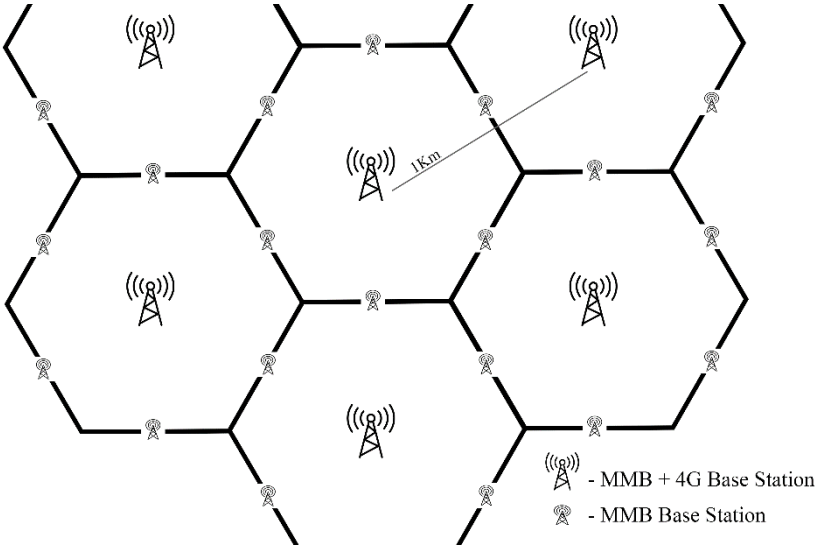

Figure 2. 1 - 5G MMB architecture

The current generation network uses the Common Public Radio Interface (CPRI) protocol to the base stations and the processing is made there. However, with the high amount of bandwidth/data promised for the next generation, it has been demonstrated in [20], the amount of data would be extremely high to use the CPRI protocol. To overcome this problem, one possible solution is a centralized network (Figure 2. 2), with the processing happening in the core, and the radio signal being optically delivered to the towers, these towers will have phased antennas arrays, needing only the optical phase

shift and demodulation to mmWave to correctly transmit the signal in the desired direction.

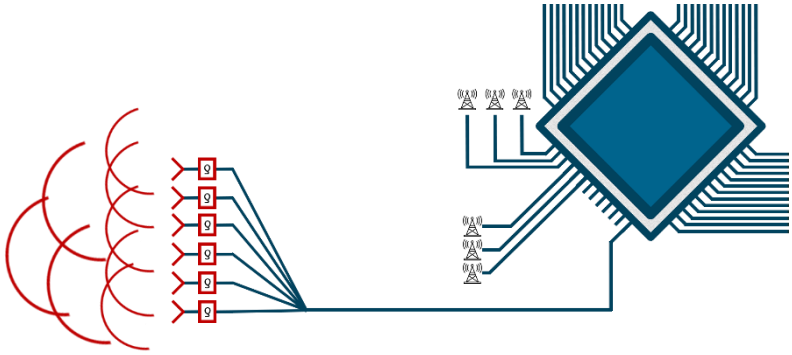

Figure 2. 2 - Centralized Network Architecture, processing is made in the core and transmits for the various towers, each tower has an array of antennas.

2.3 Applications and Requirements

Using the above architectures several case studies can be considered. One such application scenario is indoor wireless networks [3] operating in the 60 GHz band, which includes not only homes and offices, but also stadiums, museums, and shopping malls, airports, trains, stations, buses, places where it might be difficult to implement a base station or local owned network. The high bandwidth associated with the 60GHz band allows users to enjoy new technologies with high data rates and ping demands, like Virtual Reality (VR). It also allows innovative development of new internet of thing's devices and applications and having the ability to connect to higher number of bandwidth hungry devices, for example, 4k security cameras.

One service that could take full advantage of the next-generation networks is the game as a service business. Game as a service means that you pay to have access and play games, but they do not run on your computer, your computer just receives the video stream of the game and sends the inputs to the server. This technology only works well, giving the user good gaming experience, if the network latency and speed can support the service needs [22][23].

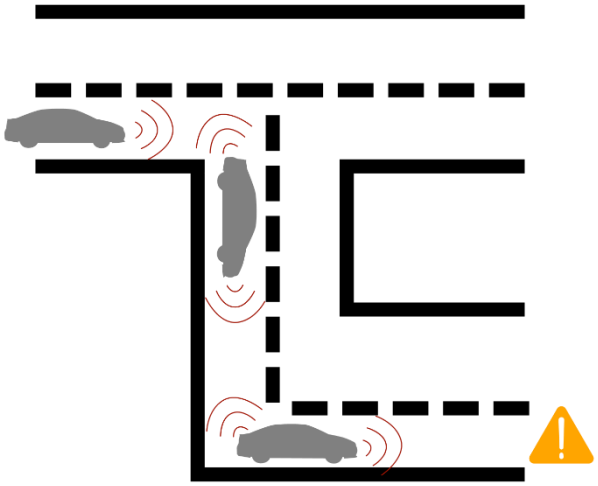

Figure 2. 3 – Example of traffic and safety benefits of cars that communicate between each other

There are also various applications in autonomous driving vehicles that are very interesting. For example, the Lidar technology, it uses the cars proximity sensors not only to map the road surrounding it but also to implement a mmWave system that sends data to other vehicles, allowing better timed warnings about dangers ahead or behind. Connected autonomous cars are a critical system that needs absolute precision, this precision can only happen if the network allows it. In other words, the networks needs to be reliable, needs to have low latency and the resources to connect every car.

3 Beam Forming and Beam Steering Concepts

3.1 Introduction

In this chapter, we present the mathematical formulation of PAAs and present beam forming and beam steering strategies based on electric phase shifter. The beam squint effect is considered, and the corresponding equivalent channel is derived. The chapter ends with a discussion of other beam steering strategies.

3.2 Mathematical Formulation of a PAA

Here we consider a receiving PAA, however the formulation can be directly applied to transmitting PAAs. Figure 3. 1 illustrates a linear array of *N* antenna elements equally spaced by the distance *d*, the signal travels different distances (Δd_i) for each element of the array (*i*), this introduces a delay to the signal that can be expressed as [24]:

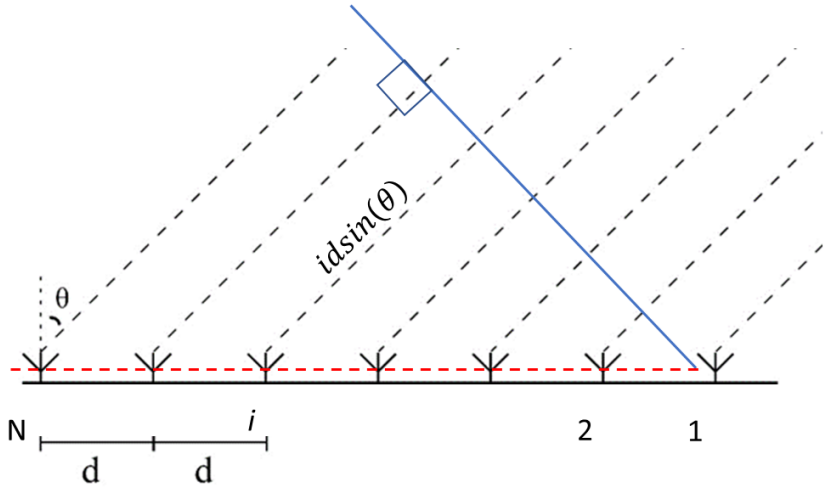

Figure 3. 1 - Uniform linear array antenna with N antenna elements, spaced uniformly

$$\Delta d_i = i\ d\ \sin(\theta)\,, i = 0, \dots, N-1 \tag{3.1}$$

$$y_i(t) = s\left(t - \frac{\Delta d_i}{c}\right), i = 0, \dots, N-1 \tag{3.2}$$

Where (y_i) is the received signal by a user for each ith antennas element and (s) is the signal that illuminates de antenna. The total received signal $y(t)$, is the vectorial sum of the signals received by all the antenna elements, equation (3.3), where *c* is the speed of light. Converting into matricial form and to the frequency domain, we obtain (2.4).

$$y(t) = \left[s(t), \dots, s\left(t - \frac{(N-1)dsin(\theta)}{c}\right)\right]^T \quad (3.3)$$

$$x(t - t_o) \longleftrightarrow X(f) = e^{-j2\pi f t_0} \quad (3.4)$$

$$y(f, \theta) = s(f)\left[1, \dots, e^{j\frac{2\pi f}{c}(N-1)d\sin(\theta)}\right]^T \quad (3.5)$$

$$y(f, \theta) = s(f)\, a(\theta, f) \quad (3.6)$$

$y(f, \theta)$ is a function of the angle of arrival (AoA), θ and $\theta \in \left[-\frac{\pi}{2}.\frac{\pi}{2}\right]$.

$a(\theta, f) = \left[1, \dots, e^{j\frac{2\pi f}{c}(N-1)d\sin(\theta)}\right]^T$ is the array factor of the PAA and can be considered as the transfer function of the system that depends on the AoA.

After the PAA, at the receiver, an optimal filter to compensate for the $a(\theta, f)$ is needed. As shown in equation (3.6) the optimal filter is composed by a sum of true time delays [11].

$$h_{optimal}(f, \theta) = a^*(\theta, f) = \left[1, \dots, e^{-j\frac{2\pi f(N-1)d\sin(\theta)}{c}}\right] \quad (3.7)$$

The array generates a delay that is compensated with the phase shift, as it is designed for the mmWave frequency, for example $f_{mW} = 60GHz$ and the desired angle of beam steering (θ_0), it will not generate the optimal compensation expressed in equation (3.6). The array delay, it comes from the difference distances between each element and the user, therefore, its delay is going to depend on the frequency of the signal received signal and the angle of the receiving user (θ).

$$h_{phase\_shift}(f_{mW}, \theta) = \left[1, \dots, e^{-j\frac{2\pi f_{mW}(N-1)d\sin(\theta_0)}{c}}\right] \quad (3.8)$$

3.3 Antenna Elements

To implement a simulation, we need the radiation pattern of a single antenna element. After evaluating the advantages and disadvantages in chapter 1.3 we picked the microstrip antenna. There are three main methods to analyse the Microstrip Antennas, transmission-line, cavity and full wave [7]. The transmission-line method is the easiest to implement, it gives good physical insight, however, it's less accurate. The Cavity method is more accurate than the transmission-line but more complex. The full wave method is the most accurate and versatile at the price of a much higher complexity. Therefore, the method chosen was the cavity method, the equations obtained for a single element rectangular path microstrip antenna were equation (3.11) and (3.12), such can be confirmed in [25]:

$$E_\theta(r,\theta,\phi) = -2Wh\left(\frac{E_0}{\mu_0}\right)\cos\phi\left(1-\Gamma^{TM}(\theta)\right)\cos\left(\frac{k_xL}{2}\right)sinc\left(\frac{k_yW}{2}\right)Tanc(k_zh) \quad (3.9)$$

$$E_\phi(r,\theta,\phi) = 2Wh\left(\frac{E_0}{\mu_0}\right)\cos\theta\sin\phi\left(1-\Gamma^{TE}(\theta)\right)\cos\left(\frac{k_xL}{2}\right)sinc\left(\frac{k_yW}{2}\right)Tanc(k_zh) \quad (3.10)$$

$$E_0 = \left(-\frac{jw\mu_0}{4\pi D}\right)^{e^{-jk_0D}} \quad (3.11)$$

$$k_x = k_0\sin\theta\cos\phi \quad (3.12)$$

$$k_y = k_0\sin\theta\sin\phi \quad (3.13)$$

$$k_z = k_0\cos\theta \quad (3.14)$$

$$1-\Gamma^{TM}(\theta) = \frac{2}{1+j(\cos\theta\sec\theta)\tan(k_0h\cos\theta)} \quad (3.15)$$

$$1-\Gamma^{TE}(\theta) = \frac{2}{1+jtan(k_0h\cos\theta)} \quad (3.16)$$

Where W and h are the dimensions of the rectangular patch, μ_0 is the free space permeability, D is the distance from the antenna to the user. In Figure 3. 2 we can see an graphic demonstration of the antenna element dimensions. This image was created using matlab's antenna design toolbox, but the design was not made by the toolbox.

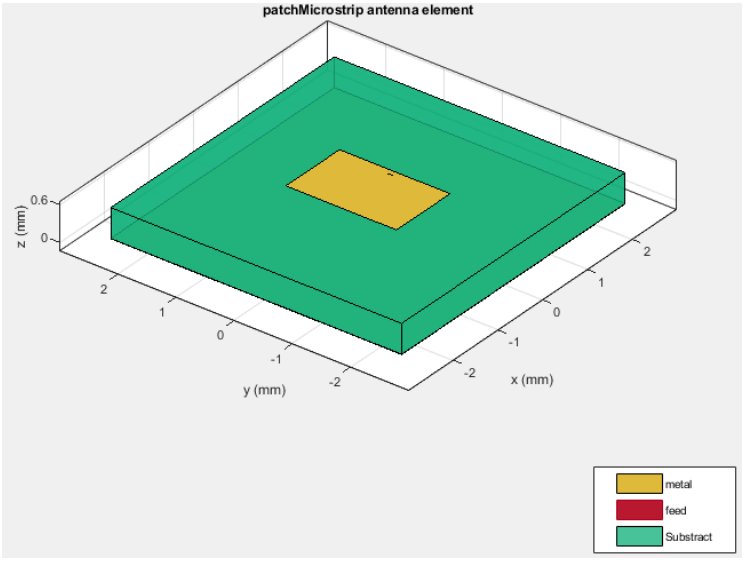

Figure 3. 2 – Antenna Element Dimensions

3.4 PAA Figures of Merit

Key Figure of Merit of PAAs are: beamwidth (BW), sidelobe level and maximum gain, which are identified in Figure 3. 3. Beamwidth is defined as the angular separation between two identical points on opposite sides of main lobe. Half power beamwidth (HPBW) is the beam width where the main lobe radiation decreases to half of the maximum, the first null beamwidth (FNBW) a is the beamwidth between the first nulls around the main lobe.

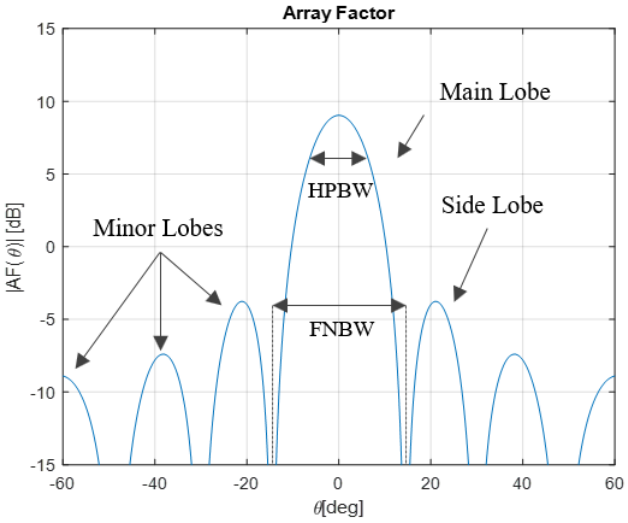

Figure 3. 3 – Array factor, lobes and beamwidth

Maximum gain or directivity describes the amount of power transmitted in the desired direction. Array gain increases with the number of elements in the PAA. Increasing the number of antennas elements decreases the HPBW and increases PAA gain and directivity as illustrated in Figure 3. 4.

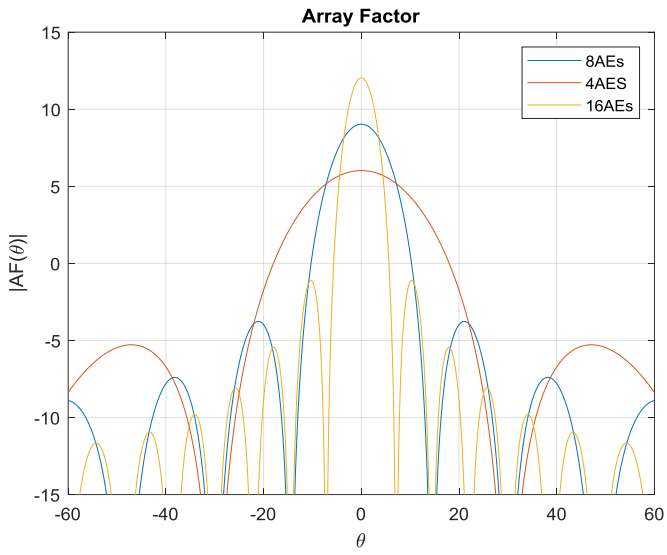

Figure 3. 4 - Directivity/gain of antenna array

3.5 Beam Forming Strategies

Beam forming is achieved in a PAA by adjusting the phase and amplitude of the signal applied to each antenna element leading to constructive interference in some directions and destructive interference in orders. There are three basic beam forming techniques.

In mmWave/analogue beamforming at the antenna site, the signal is converted from digital to analogue by the DAC and is upconverted to the mmWave frequency, where a phase shift according to the required beam direction is applied. After the mmWave is amplified by a power amplifier and feeds the AE, as illustrated in Figure 3. 5. If we consider θ_0 is the desired steering angle, the required phase shift, δ, for the n AE is given by:

$$\delta = -\beta d N cos(\theta_0) \tag{3.17}$$

$$\beta = \frac{2\pi}{\lambda} \tag{3.18}$$

The major advantages of this technique are the low cost, low complexity and low power needed to implement it because there is only one digital to analogue converter.

However, this implementation presents several problems. The phase shift for each AE is dimensioned to the carrier frequency, for high bandwidth signals, different frequency components will be affected by the phase shift dimensioned to the carrier frequency, which will result in a different delays. Hence, it is difficult to have full control of the beam direction in high bandwidth systems. Other aspects are the practical implementation of tunable phase shifters and the losses associated.

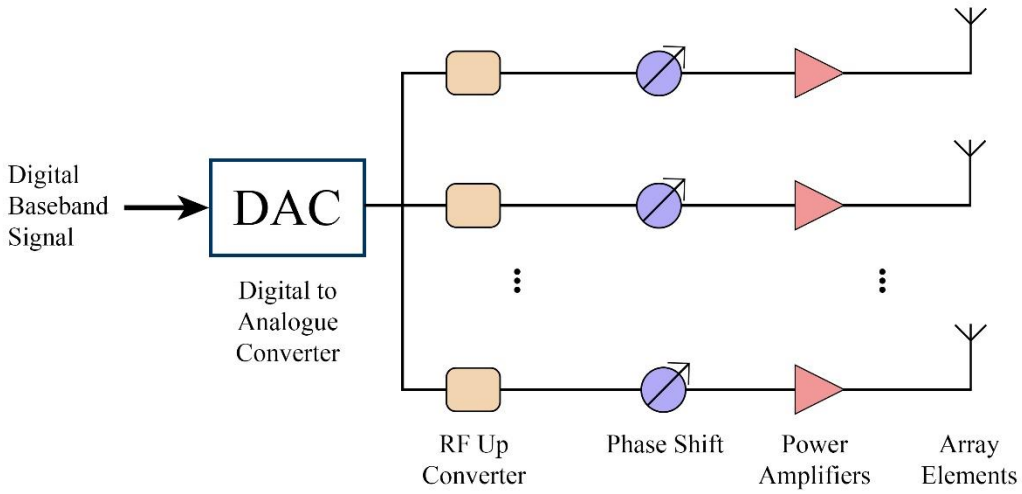

Figure 3. 5 - Analog Beamforming

In Digital Beamforming each signal individually needs to be converted from digital to analogue to realize digitally the individual processing (for example delay) for each antennas element as we can see in Figure 3. 6. This technique allows for complex processing of the signals and high bandwidth is not a problem. The disadvantages are very low cost efficient because of the high number of digital to analogue converters and high complexity, it's hard to implement because it needs processing power;

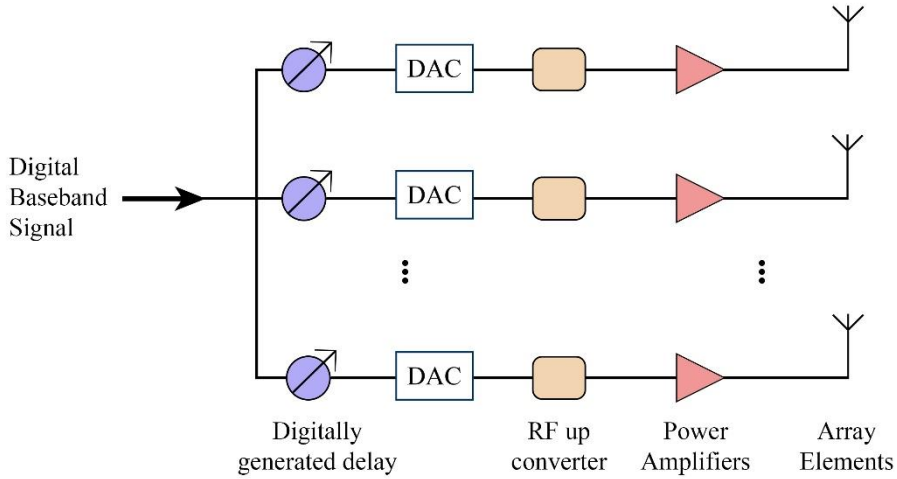

Figure 3. 6 - Digital Beam forming

In Hybrid beamforming, both technologies are conjugated to improve the analogue beamforming performance and reduce the digital beamforming complexity.

To achieve better results and taking advantage of the optic distribution of the mmWave radio signals, we are going to use a optical technioque. In this technique the signal arrives in the optical domain and the phase shift needed will be done optically, after the signal will be converted to the electrical domain and will feed the antennas elements, in this way we will have highly efficient and low complexity system without the limitations of a conventional phase shifter. In Figure 3. 7 we can see a representative diagram of the goal system, where PD is the Photo Detector.

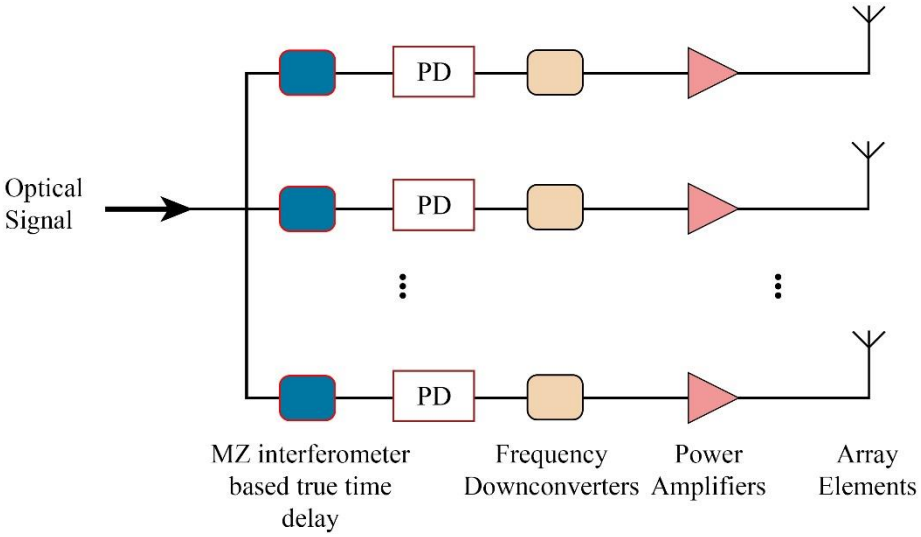

Figure 3. 7 - MZ interferometer based true time delay beamforming system

3.6 The Beam Squint Phenomenon

If a frequency independent phase shift is used to implement the $h_{phase\_shift}(f,\theta)$, i.e a phase shift $2\pi f_{mW}\frac{d}{c}\ sin(\theta_0)\ i$ is applied to the signal at the output of the antenna element i, in equation (3.7). This phase shift is calculated for f_{mW} the central frequency of the wireless signal. A signal's frequency components with a distinct frequency from f_{mW} will suffer maximum gain in a different direction and a phase distortion. As illustrated in Figure 3. 8 for a PAA of 8 antenna elements that was projected to direct an mmWave signal of 60 GHz towards 30ª. The mmWave signals of 55 GHz and 65 GHz have their maximum gain towards other directions.

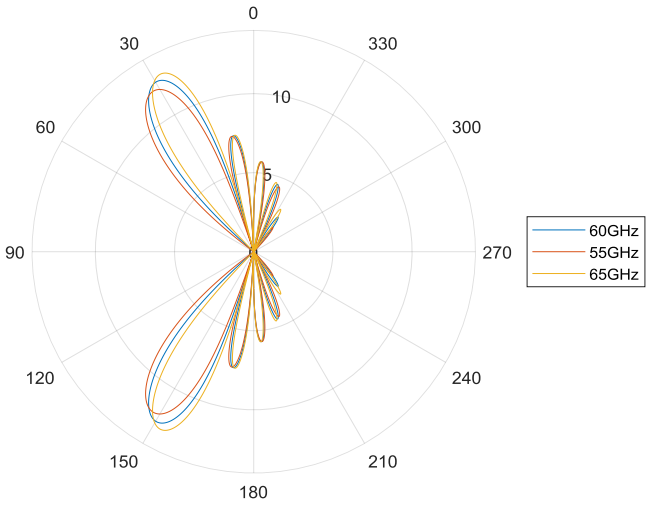

Figure 3. 8 - Differences in radiation pattern in a 60GHz system with 10GHz ofbandwidth, beam steering angle=30°.

Under this assumption the PAA gain becomes dependent on the frequency as shown in equation 3.20.

$$g(\theta_0,\theta,f,f_{mW}) = \frac{1}{\sqrt{N}} a(\theta,f) h_{phase\_shift}(f_{mW},\theta_0) = \frac{1}{\sqrt{N}} \sum_{i=0}^{N-1} e^{j\left(\frac{2\pi f\ d\ sin(\theta)\ i}{c}\right)} e^{-j\left(\frac{2\pi f_{mW}\ d\ sin(\theta_0)\ i}{c}\right)} \quad (3.19)$$

For a given AoA $\theta_0 \neq 0^{\circ}$, the PAA can be seen as a frequency selective channel, with transfer function,

$$H_{PAA}(\theta_0,\theta,f,f_{mW}) = \frac{1}{\sqrt{N}} \sum_{i=0}^{N-1} e^{j\left(\frac{2\pi f\ d\ sin(\theta_0)\ i}{c}\right)} e^{-j\left(\frac{2\pi f_{mW}\ d\ sin(\theta_0)\ i}{c}\right)} \quad (3.20)$$

$H_{PAA}(f,\theta_0)$, depends on the θ_0 and the number of antenna elements. Illustrated in Figure 3. 9 and Figure 3. 10 is the equivalent channel bandwidth. The bandwidth decreases as the number of antenna elements increases and the same trend is observed when the AoA increases. Therefore, there is a compromise between the PAA bandwidth and gain. The phase compensation is only achieved for the mmWave carrier, failing to compensate for the adjacent frequencies as it is illustrated in the right side of Figure 3. 9 and Figure 3. 10. The higher the number of antennas or the angle of beam steering the higher is the slope of the phase, meaning higher losses for adjacent frequencies of the mmWave carrier.

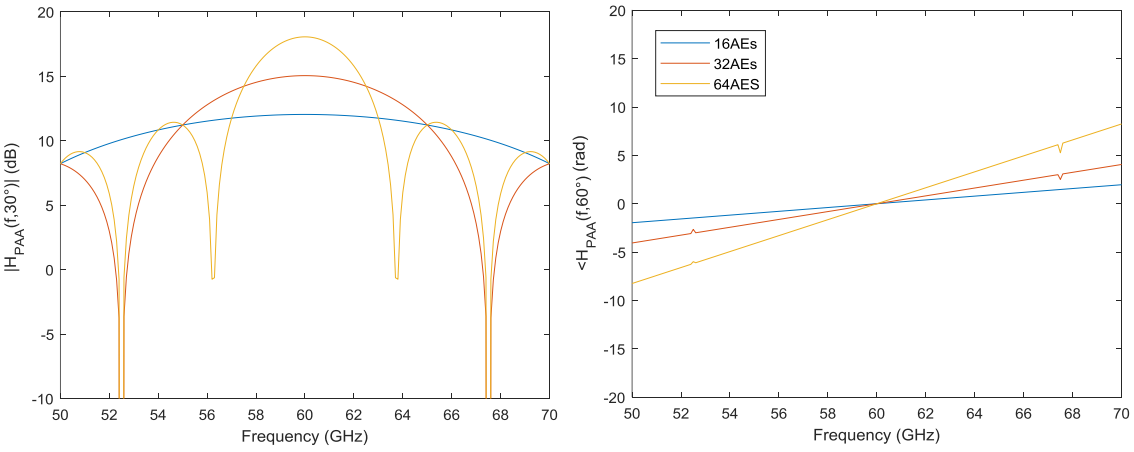

Figure 3. 9 - Transfer Function of a PAA for 30 degrees of beam steering (left) absolute value (right) phase difference to the mmWave carrier

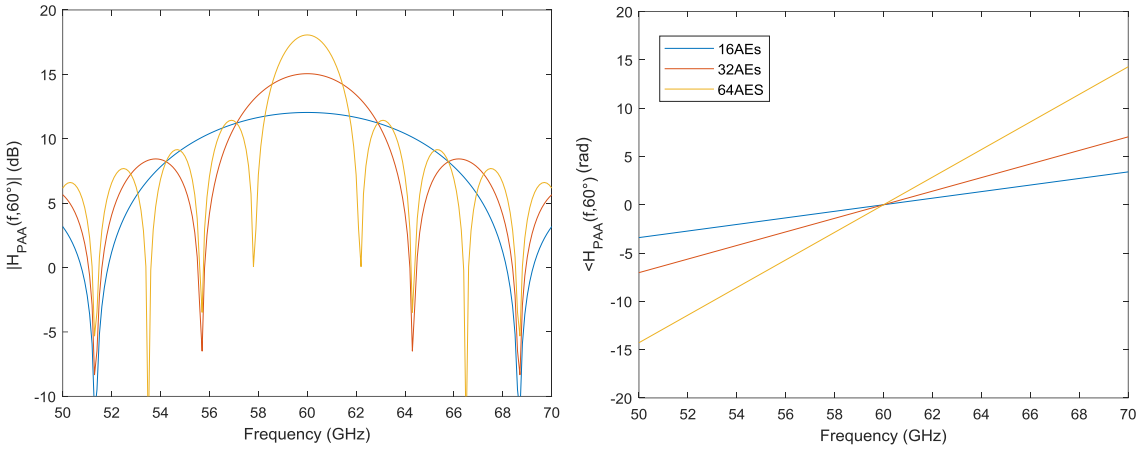

Figure 3. 10 - Transfer Function of a PAA for 60 degrees of beam steering

3.7 Other Beam Steering Methods

Beam steering consists of steering the main lobe of an antenna system's radiation pattern. There are many methods to achieve beam steering [26]:

- Mechanical beam steering – in this method beam steering is achieved turning physically the antenna element(s) to direct the maximum lobe to the desired direction. The main advantage of this method is the maximum lobe will always have the same gain for every angle of beam steering, the disadvantage is the need to implements a mechanical system to every antennas array which adds more complexity and points of failure;

- Beamforming – it combines the radiation from various antennas from an array constructively in a desired direction using phased arrays. The main advantage of this method is its low complexity, needing just a phase-shifter per antenna element of the array and no moving parts are necessary. The disadvantage is that the main lobe will not have the same gain for all the angles of beam steering because of the nature of the antenna's element radiation and the steering angle control may be difficult;

- Reflectarray antennas – this technique combines an antenna array and reflectors to achieve the beam steering directing the beam using the reflector. The beam is directed to numerous reflectors equally spaced, each reflector reflects a different direction, by small deviations of the beam we can steer the beam. This can also be achieved with an active element, bringing all the disadvantages of it. One of the main advantages of this method is the gain of the main lobe that will not reduce as much as in the beamforming method with higher angles of beam steering, the fact that for

mmWave's systems it's lightweight and the possibility to have multiple beams in different directions supporting point-to-multipoint applications. The disadvantage is the fact that it needs one active element to steer the beam continuously to different directions, and if an active element is not being used, then it will not allow for continuous control of the beam's direction;

- Parasitic Steering – this principle is based on Yagi-Uda antennas[7], these antennas consist of one exited element and other parasitic elements, the ones behind the exited one are called reflectors and the ones in front are called directors. The directors are shorted to the ground and, as the name implies, direct the radiation and the reflectors are an open circuit and reflect it. To achieve beam steering an Electrically Steerable Passive Array Radiators (ESPAR) was created, it has a central driven element and is surrounded by parasite elements that can be grounded or an open circuit as desired, thus allowing the control of the beam's direction. Parasitic steering has been achieved using microstrip antennas with a $\pm 30°$ of steering. This method as the advantage of not decreasing the bandwidth as much as beamforming, the beam gain by changing its direction. The disadvantages are its complexity, it needs to have switches or variable reactors to connect or disconnect the parasite elements to the ground, and the control of the beam's direction is not continuous and its step depends on the number of parasitic elements;

- Integrated Lens Antennas (ILA) – are constituted by an antenna array and a lens that has the focal point for each antenna element in the middle, therefore, controlling which antenna element is radiating with a switch allows us to control the direction of the main beam, as we can see in the Figure 3. 11. This system has clear disadvantages, the gain of the radiation pattern will not be as directive meaning it will have less gain in the main lobe and the control of the angles of beam steering is not linear and has as many steps as the number of elements. One advantage is the gain does not decrease with a higher angle of beam steering.

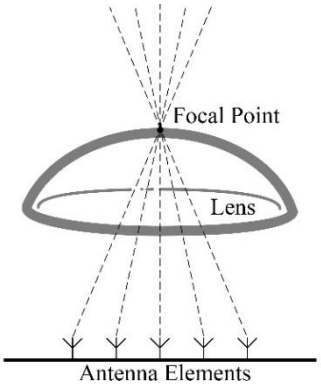

Figure 3. 11 - Integrated lens antennas

- Switched Beam Antenna (SBA) – various antennas elements arranged to cover various directions, each one is directed to a specific direction, with a switch we can control which antennas element is radiating and choosing the desired antenna we steer the beam. As it is very similar to the integrated lens antenna this technique has the same flaws, the gain of the radiation pattern will not be as directive, meaning it will have less gain in the main lobe and the control of the angles of beam steering is not linear and it has many steps as the number of elements , the advantage is that the gain doesn't change with the angle of beam steering and it doesn't need the lens, but a structure with antennas elements.

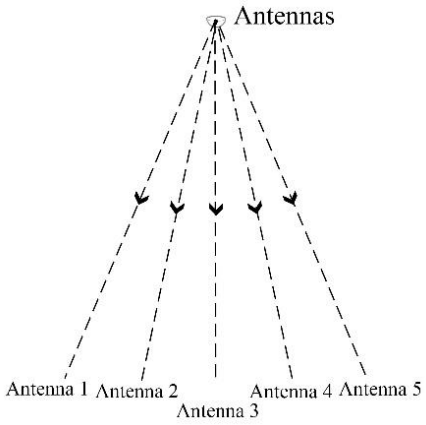

Figure 3. 12 - Switched Beam Antenna

- Traveling Wave Antennas (TWA) – in these antennas the current travels in only one direction and acts as a radiating mechanism, in opposition to resonant antennas. The advantage is higher bandwidth, it radiates at all the frequencies in the operation bandwidth, different frequencies mean different angles, however, there are other ways to steer the beam for a chosen frequency:
    - Dual feeding points;
    - Parasitic effect/Slot loading – with the antennas surrounded by patches, controlling which patches are grounded using switches allows to control the reactance around the antenna, controlling the beam direction;
    - Using materials with adjustable properties.

  However, the problem associated with high bandwidth system is also present in this technique, if different frequencies mean different steering

angles, even using one of the three steering techniques to steer the beam for a given frequency, a signal with a high enough bandwidth will have different angles for different frequency components.

- Retrodirective Arrays – this antenna's system is based on the corner reflector principle, meaning it can redirect a signal towards the source without any previous information about its location. There are two main types of retrodirective antennas:
    - Van Atta array – using connected antenna pairs, one receives the signal and the other re-transmits the phased signal towards the source. It uses the transmission line principle to achieve the phase reversing of the signal and the transmitting antennas redirect the beam back to the source;

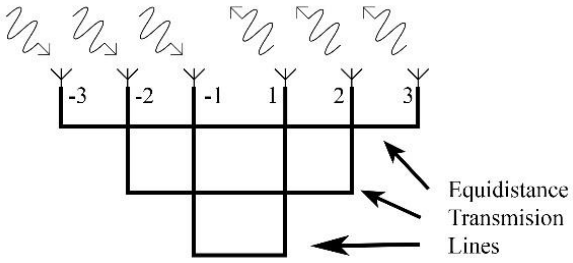

Figure 3. 13 - Van Atta Array

    - Phase Conjugating Mixers – the phase inversion is achieved using a heterodyne technique with mixers and a local oscillator, with this technique we can use the same antenna to receive and transmit;

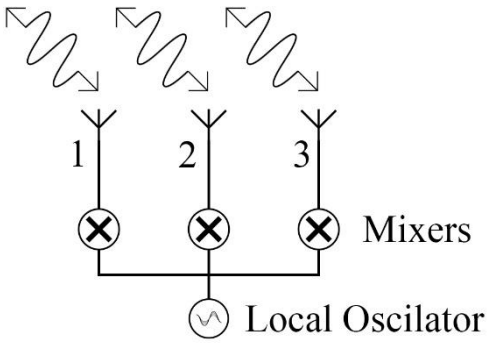

Figure 3. 14 - Phase Conjugating Mixers

There other ways to achieve the phasing of the signal with improved performance, like phase detection and digital techniques however, they also add more complexity.

Retrodirective Arrays can be very useful for the mobile devices that connect to the antenna's tower because they can transmit to the direction of the tower with a low complexity system. The disadvantage of this system is that it can receive other signals and change the direction of the transmit signal missing the objective (source);

- Metamaterial Antenna – a metamaterial is a man-made material developed to have electromagnetically proprieties that cannot be found in natural materials. Changing the antenna's active material proprieties like permittivity and permeability, we can steer the beam. This allows for a less complex system to achieve beam steering. However, the building process is extremely complex and difficult;

With all these technique's information, a summary table was made to analyse and compare the methods in a more pleasantly and compact way. The chosen characteristics to compare the systems where the Insertion Loss (IL), Steering Resolution (S-Res), the complexity, the Bandwidth phase deviation (BPD), the size and the cost of each technique respective system.

Technique	IL	S-Res	Complexity	BPD	Size	Cost
Mechanical	*None*	*Continuous*	*Low*	*None*	*Large*	*Low*
BF	*High*	*Predefined*	*Moderate*	*High*	*Medium*	*High*
Reflectarray	*Medium*	*Predefined*	*Moderate*	*High*	*Large*	*High*
Parasitic	*Low*	*Predefined*	*Low*	-	*Freq-dependent*	*Low*
ILA	*Low*	*Predefined*	*Low*	-	*Medium*	*Low*
SBA	*Medium*	*Predefined*	*Low*	*None*	*Large*	*High*
TWA	*None*	*Continuous*	*Low*	*High*	*Small*	*Low*
R-Arrays	*Low*	*Fine*	*Moderate*	-	*Medium*	*Medium*
Metamaterial	*High*	*Predefined*	*Moderate*	-	*Medium*	*Medium*

Table 1 – Summary of Beam steering techniques characteristics.

After analysing the Table 1, the chosen beam steering method for this work was Beamforming because of its acceptable complexity but intending to achieve a final system that has low complexity but beyond acceptable figures of merit.

4 Influence of Beam Squint on System Performance

4.1 Introduction

In this chapter we introduce the simulation system model. The beam steering is performed by means of electric phase shifters, which are dimensioned for the mmWave carrier. The effect of beam squint on system performance is analysed for different operating conditions. The performance of the system is evaluated in terms of Error Vector Magnitude (EVM). To compensate the beam squint effect we apply a baseband digital compensation strategy. The digital compensation strategy proves to compensate efficiently the beam squint effect, however, it fails for situations where the relative delay introduced by the antenna elements increases above a certain limit.

4.2 System Model

Figure 4. 1 depicts the simplified diagram of the wireless system that will be considered in this chapter. The system employs beam steering both in the transmitter (TX) and receiver (RX) employing tunable phase shifter that controls the phase of the signals of each antenna element. In the transmitter, the digital signal is processed digitally and is converted to the analogic domain by a digital to analogue converter (DAC). After the baseband signal is up-converted to the desired mmWave frequency band. The mmWave signal is then distributed to the antenna elements with the appropriate phase shift. In the receiver side (RX) the PAA is pointed toward a given direction, which is adjusted by the analogue phase shifters. The mmWave signals from the AE elements are combined, down-converted and digitalized by the analogue to digital converter (ADC). After digitalization, the signal can be processed. We can identify three functional blocks: the digital block, the mmWave chain and the PAA.

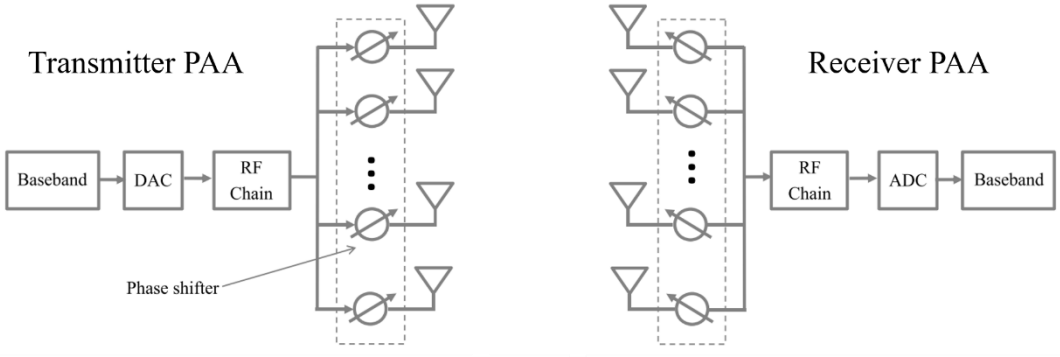

Figure 4. 1 - System model diagram, image adapted from [24]

Chapter 2 was dedicated to PAAs in this chapter we will considerer the digital and mmWave functional blocks.

4.2.1 Mathematical formulation of OFDM signals

The wireless signal considered is an Orthogonal Frequency Division Multiplexing (OFDM) signal. This data modulation technique uses several orthogonal subcarriers that are modulated with the data. Being composed of N equally spaced orthogonal subcarriers spaced by the frequency, $\Delta f = \frac{1}{T_{sym}}$, where $T_{sym}$is the duration of an OFDM symbol. The l^{th} OFDM symbol can be expressed as a function of time as:

$$x_l(t) = \frac{1}{T_{sym}} \sum_{k=0}^{N-1} X_l[k] e^{j2\pi f_k (t - lT_{sym})} \tag{4.1}$$

The frequency of subcarrier k is given by $f_k = k/T_{sym}$, where $k = 0,1..N-1$. The l^{th} symbol transmitted by the subcarrier k is denoted by $X_l[k]$.

When sampling at $x_l(t)$ at $t = lT_{sym} + nT_s$, where $T_s = T_{sym}/N$, results in the sampled signal $x_l[n]$

$$x_l[n] = \sum_{k=0}^{N-1} X_l[k] e^{j2\pi kn/N} \tag{4.2}$$

Equation (4.2) shows that this modulation technique can be implemented in digital signal processing using the Inverse Fast Fourier Transform (IFFT).
Identically, the demodulation of an OFDM symbol is equivalent to the Discrete Fourier Transform (DFT) and can be implemented using the Fast Fourier Transform (FFT). Denoting the received symbol as $y_l[n]$, the received signal is given by Equation 4.3.

$$Y_l[k] = \sum_{n=0}^{N-1} y_l[n] e^{-j2\pi kn/N} \tag{4.3}$$

4.2.2 The Cyclic Prefix

In dispersive channels, such as optical fiber transmission and wireless multipath fading, the signal spreads along time. This can be problematic if a certain OFDM symbol crosses its boundary and causes interference with another OFDM symbol. To avoid this problem to a cyclic extension of the symbol itself is added to the OFDM symbol, which is called a cyclic prefix (CP).

4.2.3 OFDM Signal Generator and mmWave up conversion

Figure 4. 2 illustrates the schematic diagram of an mmWave OFDM generator. The binary data string is divided into parallel blocks of *N* sub-strings and each parallel sub-string is

mapped into a mQAM symbol. The N blocks of QAM symbols are sent to the IFFT block. After the IFFT data is converted from parallel to serial and the CP is added. All these operations can be performed by digital signal processing. Next, data is converted to the analog domain by a digital to analog converter (DAC). To eliminate the aliasing components introduced by the DAC, a low pass filter (LPF) is used. The LPF can also be used for signal shaping, here we consider a square root raised cosine filter. After the LPF, the signals are up-converted to the specified mmWave frequency f_c, this process is mathematically described as:

$$x_{RF}(t) = x_I cos(2\pi f_c t) + x_Q sin(2\pi f_c t) \quad (4.4)$$

Where x_I and x_Q are the low-pass filtered real and imaginary components of the OFDM baseband signal. After that, the signal is amplified and transmitted through a phased array antenna.

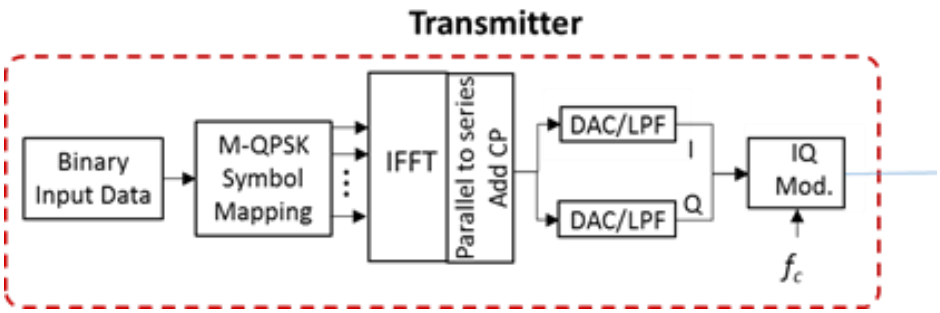

Figure 4. 2 - mmWave OFDM generator

4.2.4 OFDM Receiver

The OFDM receiver depicted in Figure 4. 3 performs all the inverse operations of the transmitter, here we consider the uses an equalizer to compensate for amplitude and phase distortion introduced by the system components, including antenna arrays and channel transmission. The equalizer is calculated with the initial test string that allows us to calculate the system frequency response and compensate it to receive the correct data.

This test string is sent initially but it needs to be repeated over time to compensate for the possible changes that happen to the channel (like changing weather conditions).

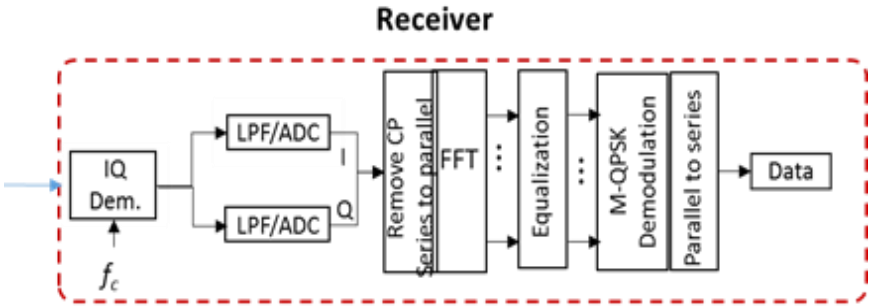

Figure 4. 3 - mmWave OFDM Receiver

4.2.5 Transmitter Digital Equalizer

In this work, we consider a digital equalizer that is evaluated using training sequences of transmitted OFDM symbols in each subcarrier $X_l = [X[0], X[1], \dots, X[N_l - 1]]$ $\boldsymbol{X_l} = [X[0], X[1], \cdots, X[N-1]]$. The received signal, $Y[k]Y[k]$, at each subcarrier $k = 0, \dots, N_l - 1$, can be expressed as:

$$Y[k] = X[k]H[k] + n[k] \tag{4.5}$$

where denotes $H[k]$ $H[k]$ the system's frequency response at k_{th} sub-carrier and $n[k]$ $n[k]$ represents the complex additive white gaussian noise (AWGN) sample introduced by the system. Using vectoral representation $Y_l = [Y[0], Y[1], \dots, Y[N_l - 1]]$ $\boldsymbol{Y_l} = [Y[0], Y[1], \cdots, Y[N-1]]$ and $H = [K[0], H[1], \dots, H[N_l - 1]]$ $\boldsymbol{H} = [H[0], H[1], \cdots, Y[N-1]]$ and assuming, that the noise introduced by the system is negligible,

$$Y = XH^T \tag{4.6}$$

Where $[\,]^T[\quad]^T$ denotes the transposed vector. The equalizer $H_{eq}\boldsymbol{H_{eq}}$, that compensates the system response,

$$YH_{eq}^T = XH^T H_{eq}^T = X \tag{4.7}$$

The estimate of the system equalizer can be calculated as:

$$H_{eq}^T = XY^{-1} \tag{4.8}$$

$\boldsymbol{H_{eq}}\boldsymbol{H_{eq}}$ can be calculated for each OFDM subcarrier as:

$$H_{eq} = \frac{Y[k]}{X[k]} \tag{4.9}$$

A training sequence composed of N_t OFDM symbols is transmitted at the beginning of the transmission. Training symbols are symbols chosen at the beginning of the transmission. Owing to the noise introduced in the system, more than one OFDM training symbol is required to properly remove the noise from the estimation. Therefore, for each subcarrier, the equalizer term is calculated as:

$$H_{eq} = \frac{1}{N_t} \sum_{n=1}^{N_l} \frac{Y_n[k]}{X_n[k]} \tag{4.10}$$

Where $Y_{k,n}$ $Y_{k,n}$ and $X_{k,n}$ $X_{k,n}$ are the received and transmitted symbols at the k^{th} subcarrier of the n^{th} symbol.

4.2.6 Digital Modulation

Each one of the OFDM carriers as modulated data with the Quadrature Amplitude Modulation (QAM). This modulation organizes the bits into symbols creating a constellation. Depending on the chosen QAM order we will have a respective number of symbols, for example in 16QAM we will have 16 symbols and $\log_2 16 = 4$ bits per symbol. The higher the QAM order, the higher amount of information can be sent in less bandwidth, however, the bit error rate (BER) will be higher because the distance between symbols will be lower, meaning that with a lower amount of noise the symbols can be misinterpreted, this can be seen in the Figure 4. 4. To modulate the constellation, QAM takes advantages of the proprieties of two orthogonal carriers, allowing to modulate different data into the two carriers and send it all together. Taking advantage of the orthogonality we will always be able to recover the separate data from each orthogonal carrier.

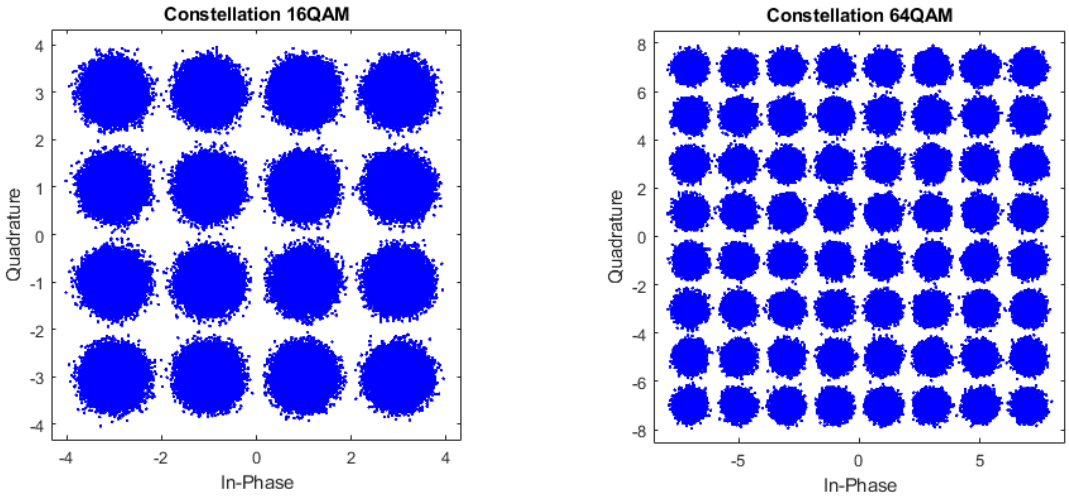

Figure 4. 4 - Constellations od 16 and 64 QAM clear difference in symbols distances

4.3 System Performance Metrics

Error Vector Magnitude (EVM) is a system's performance indicator that measures the distance vectors between the optimal constellation and the received.

EVM can be expressed in percentage of the root-mean-square (RMS), according to:

$$EVM_{rms}(\%) = \left[\frac{\frac{1}{N_l}\sum_{k=1}^{N_l}|Y_k - X_k|^2}{\frac{1}{N_l}\sum_{k=1}^{N_l}|X_k|^2}\right]^{\frac{1}{2}} \times 100 \tag{4.11}$$

Where $Y_k = Y_{(l,k)} + iY_{Q,k}$ $Y_k = Y_{I,k} + iY_{Q,k}$ is the k^{th} actual received symbol and$X_k = X_{l,k} + iX_{Q,k}$, is the ideal transmitted symbol and N_l is the number of carriers. The principal advantage of this method is that we can evaluate a system without knowing what is being transmitted.

Bit Error Rate (BER) represents the probability of an error occurring when deciding what bit was transmitted. To measure BER particularly for systems with low BER long sequences must be used. However, BER can be defined as a function of theEVM_{RMS} EVM_{RMS}, according to [27] as:

$$P_b \approx \frac{2\left(1-\frac{1}{L}\right)}{\log_2 L} Q\left[\sqrt{\left(\frac{3\log_2 L}{L^2-1}\right)\frac{2}{EVM_{RMS}^2 \log_2 M}}\right] \tag{4.12}$$

Where L is the number of levels in each dimension of the constellation, M is the number of symbols and Q[.] is the Gaussian co-error function.

Although BER is a more precise performance metric, several standards such as [28] employ EVM as the required performance metric. Examples of the system EVM requirements for different modulation schemes are given in Table 2.

Table 2 - Error vector magnitude specification for Wide Area BS

Wide Area Base Station according to TS36.104	
Modulation Scheme	Required EVM [%]
QPSK	17.5%
16 QAM	12.5%
64 QAM	8%

4.4 System Simulation Model

This simulation starts, as depicted in Figure 4. 5, with the generation of the digital OFDM signal, then the signal is converted to analogue and upconverted to the mmWave frequency to feed the PAA.

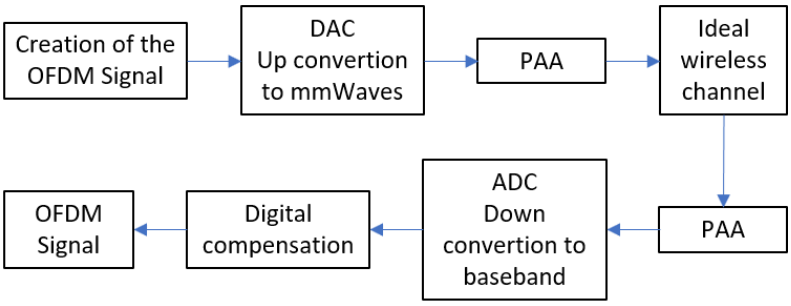

Figure 4. 5 - Block Diagram of the simulation model

Using the array factor and the Radiation Pattern of a single element we created the radiation pattern of the PAA in the same way we created the one for a single element, creating a matrix with all the angles for all the frequencies of the frequency vector. This allows us to simulate correctly the effect of beam squint in an OFDM system, choosing an angle we can multiply the radiation pattern's frequency response by the OFDM signal in the frequency domain simulating the transmission.

The digital compensation is achieved using a known bit sequence initially calculating the constellation phase delay and compensating it in the actual transmission.

4.5 System Simulation Parameters

Operation in the 60 GHz and 20 GHz regions is considered, and the radio channel was considered ideal. The OFDM signal is composed of 32 equally-spaced orthogonal subcarriers and a cyclic prefix of 25%. Square root raised cosine filters, with a roll-off factor of 25% are considered both at the transmitter and receiver.

The system parameters that are changed along the following analysis are the number of antenna elements, bit rate, and constellation order.

4.6 Beam Squint Effect versus Signal Bandwidth

Figure 4. 6 shows the EVM versus the beam steering angle, considering the bit rates of: 5Gbit/s, 7.5 Gbit/s, 12.5 Gbit/s and 15 Gbit/s. 4QAM modulation is employed and the number of the antenna elements is 16.

According to Table 2 the maximum percentage of EVM is 17.5%. This value is represented in the graph as a red dashed line.

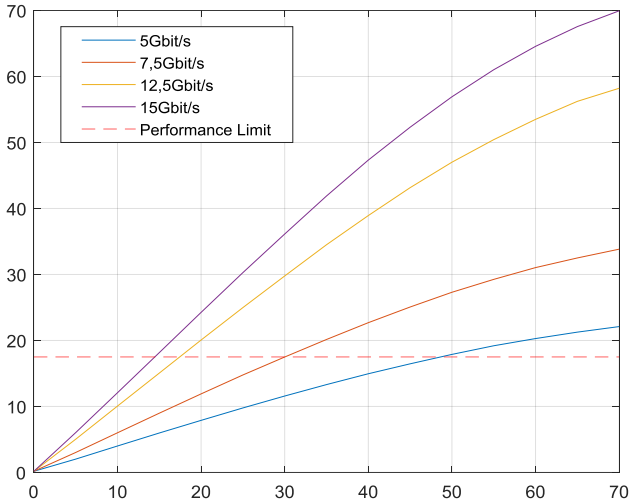

Figure 4. 6 - EVM variation with the bitrate

By increasing the bitrate, the bandwidth of the signal also increases, this causes the squint effect to be more noticeable as we can see in the Figure 4. 6. The system with 5Gbit/s can steer the beam until 48º below minimum performance. Increasing the bit rate will decrease the maximum angle supported. The system with 7.5Gbit/s allows up to a 30º steer, the 12.5Gbit/s allows 17º and the 15Gbit/s only allows for a 14º steer.

4.7 Beam Squint Effect versus Number of Antenna Elements

Figure 4. 7 shows how the numbers of AEs affect the EVM of the system as a function of the beam steering angle. The following numbers of AEs were considered: 4, 8, 16 and 32. 4QAM modulation is employed and the bitrate is 5Gbit/s.

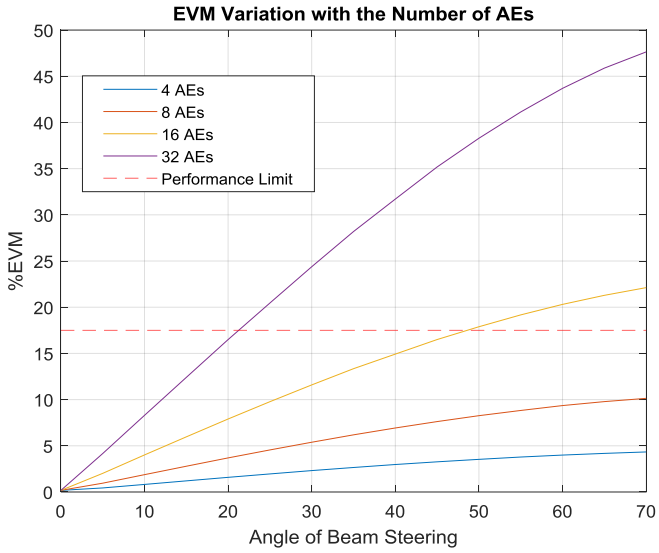

Figure 4. 7 - EVM variation with AEs

Increasing the number of AEs we increase the directivity and gain of the beam, therefore, the system is going to be more robust to losses. However, we also add more complexity, there are more antennas and more different paths with different distances to the user. In this simulation, we consider a perfect channel so when we increase the number of antennas, we are only going to increase the interference and obtain increasingly worst EVMs. For 4 and 8 AEs the system can steer the beam to the 70º without getting below the minimum performance requirement, but the 16 AEs system stops at 48 and the 32 AEs system stops at 22º.

4.8 Beam Squint versus Modulation Scheme

Following the same strategy as before, we are going to calculate the EVM as a function of the beam steering angle, at this time we are going to vary the modulation order. In the Figure 4. 8 we can see the EVM percentage for 4, 8, 16, 32 and 64 QAM for a system with 16 AEs and the 5Gbit/s bitrate. The minimum performance is not present now because the minimum performance varies with the modulation order as it was described in Table 2.

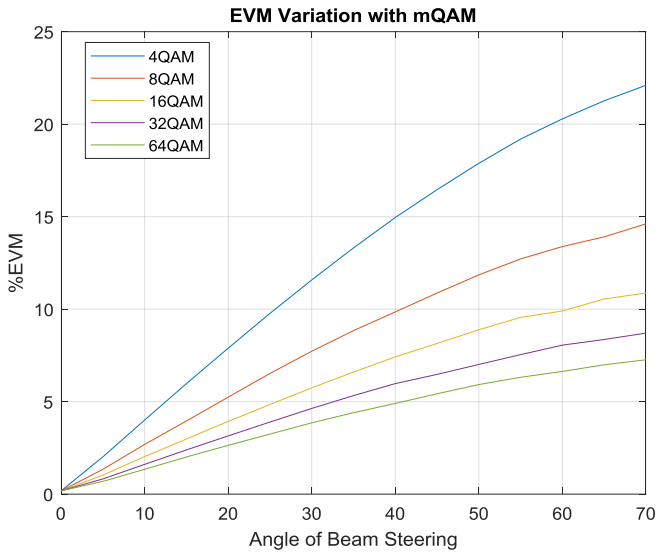

Figure 4. 8 - EVM variation with QAM modulation order

As we can see in the Figure that when we increase the *m* value of the mQAM modulation we increase the number of symbols, reducing the bandwidth and the beam squint effect. In our simulation, the EVM values decrease with the increasing of the *m* value because we have a perfect system without noise and for higher values of *m* the signal occupies a smaller bandwidth. In a real system, the expected EVM evolution was to get better until a certain value of m and then as we increase m further the EVM would get worse.

4.9 Baseband Digital Beam Squint Compensation

The baseband digital compensation is achieved sending a known signal to the receiver to test the channel and calculate the phase and amplitude differences between the sent and received constellations. This difference is used in the communication to correct the phase differences improving signal quality and consequently the EVM.

In Figure 4. 9 shows the received constellation with squint effect for a system with 4QAM, 16 AEs and 5Gbit/s, the constellation suffers from rotations, that translate in phase constant phase differences, and from power losses because of the different gain associated with the different frequencies components. The phase difference, being constant, can be calculated to restore the constellation.

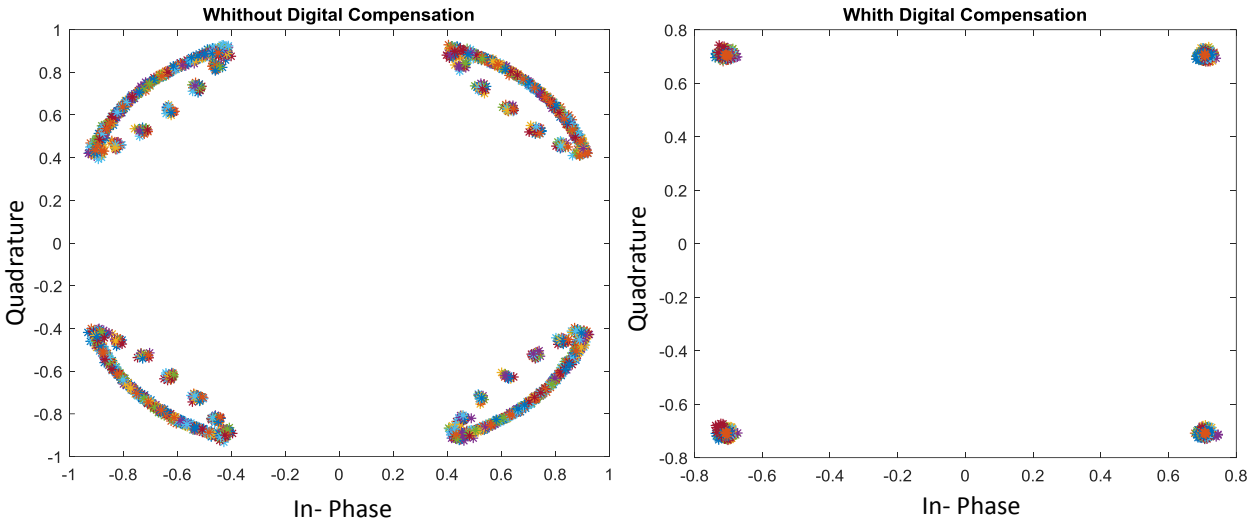

Figure 4. 9 - Constellation without(left) and with(right) digital compensation

With this equalization, we can fully recover the signal improving very significantly the EVM of the system as it is shown in Figure 4. 10.

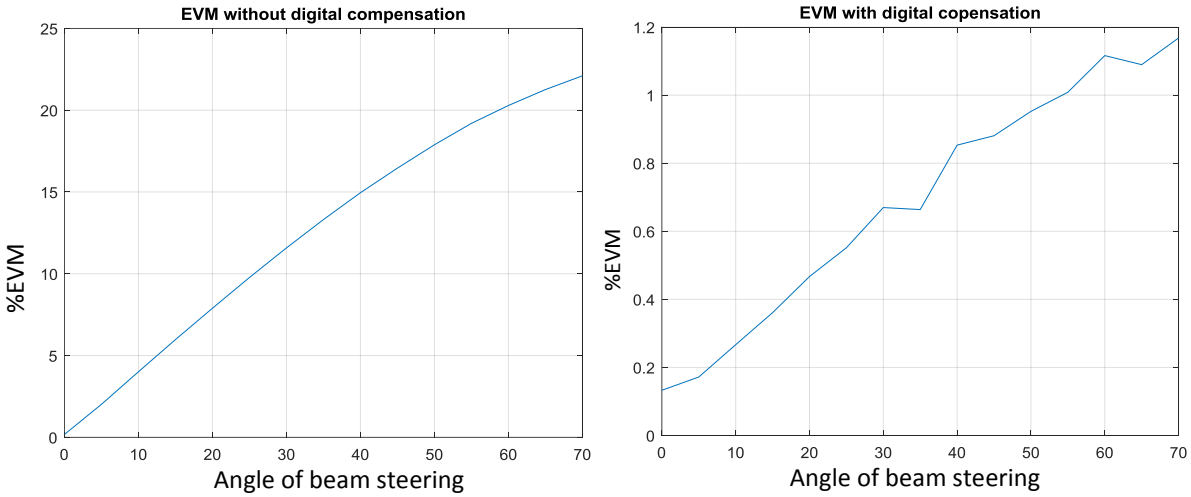

Figure 4. 10 - EVM without(left) and with(right) digital compensation

To see the full potential of the digital compensation, Figure 4. 11 shows the worst EVM and its correction. The system is the one with 15Gbit/s and its constellation loses some point, however, we can still recover it.

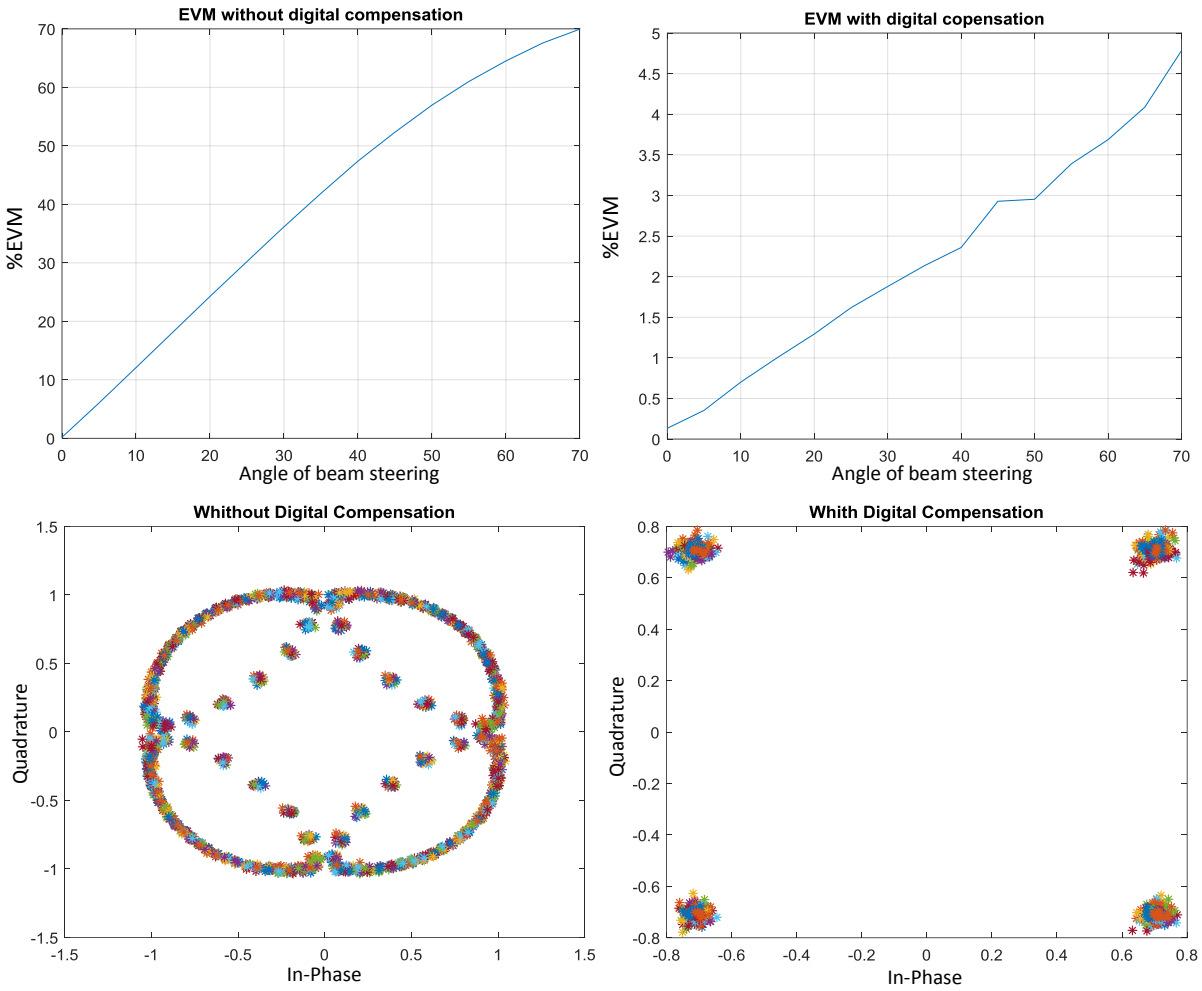

Figure 4. 11 - EVM and constellations of the 15Gbit/s system with(right) and without(left) digital correction

The constellations have not only suffered phase distortion but also power distortion. In the optical domain, the carriers from the borders of the OFDM signal have less power, those are the ones closer to the middle, and in the electrical domain, the phase shift introduces most of the phase differences causing it to rotate. Based on these results we can simulate the transfer functions needed to almost fully compensate these distortions.

To test the limitations of the digital compensation we are going to run a simulation with isotropic antennas where we increase the number of antennas to a point where the digital compensation is not able to recover the distortions. Using mmWaves the frequency is high therefore we need to increase the number of antennas up to 128 elements, this creates a computational heavy simulation. To better show this effect we decreased the frequency of the mmWave carrier frequency and simulated the effect in omnidirectional antennas. By decreasing the frequency, we are increasing the wavelength of the signal, this allows for greater phase shifts with smaller distances, therefore, higher distortions with less elements.

In the Figure 4. 12 e Figure 4. 13 we will see that for 60GHz the digital compensation only fails for 128 elements and for 20GHz it starts to fail for 32 elements. In these situations, the distortion has to be compensated with photonic methods.

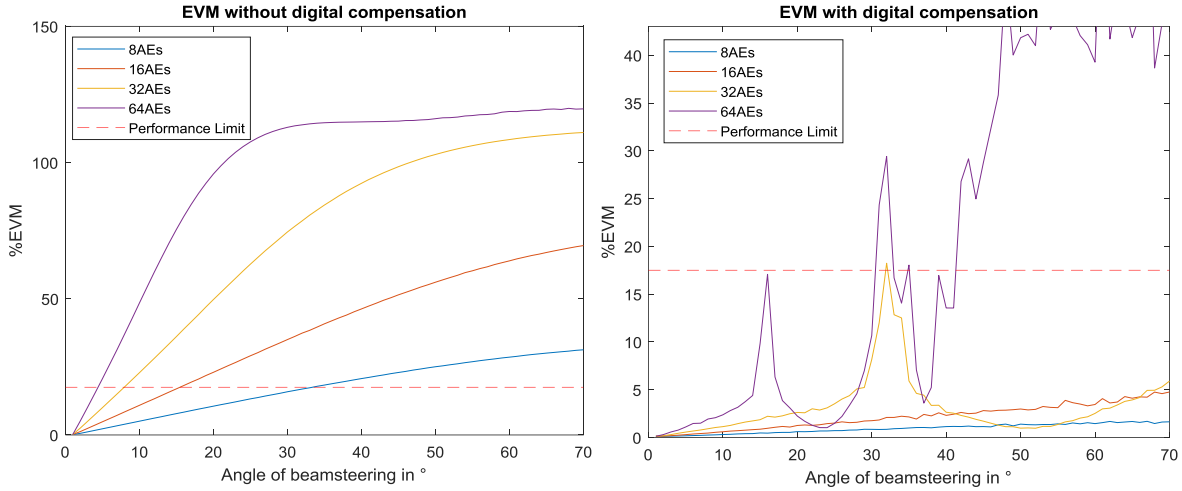

Figure 4. 12 - EVM variation with AEs at 20GHz

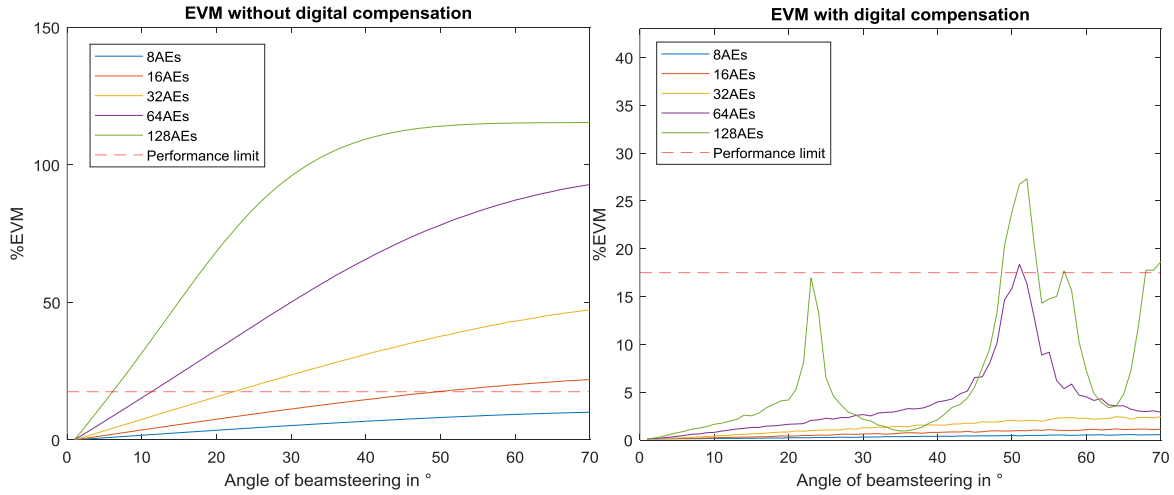

Figure 4. 13 - EVM variation with AEs at 60GHz

5 Photonic Beam Steering Techniques

5.1 Introduction

Traditional phased array antennas that rely on bandwidth limited radio frequency phase shifters originate the beam-squint problem. True-time-delay (TTD) beamforming based on low-loss photonic delay lines can solve this problem [18]. In this chapter a simulation model to evaluate photonic beam steering will be presented. A photonic beam steering strategy based on a continuously tunable Mach–Zehnder Interferometer (CT-MZI) will be evaluated assessing the possibility of a photonic beam steering compensation system overcoming the limitations of electric phase shifter and baseband digital compensation.

5.2 Photonic Beam Steering Systems

The photonic supported beam steering follows similar beam steering principles as its electrical counterpart, however the phases of the signals from the different antenna elements are processed in the optical domain. In this case, the signals of the antenna elements of a receiving PAA must first be converted into optical signals by means of optical modulation, and then their phase is controlled in the optical domain and combined by means of an optical coupler, and eventually the output is optically transmitted to the network core, where the signal is processed. For transmitting antennas, the signal stream is inverted, and the orders of electro-optical (E/O) and opto-electrical (O/E) conversion are reversed.

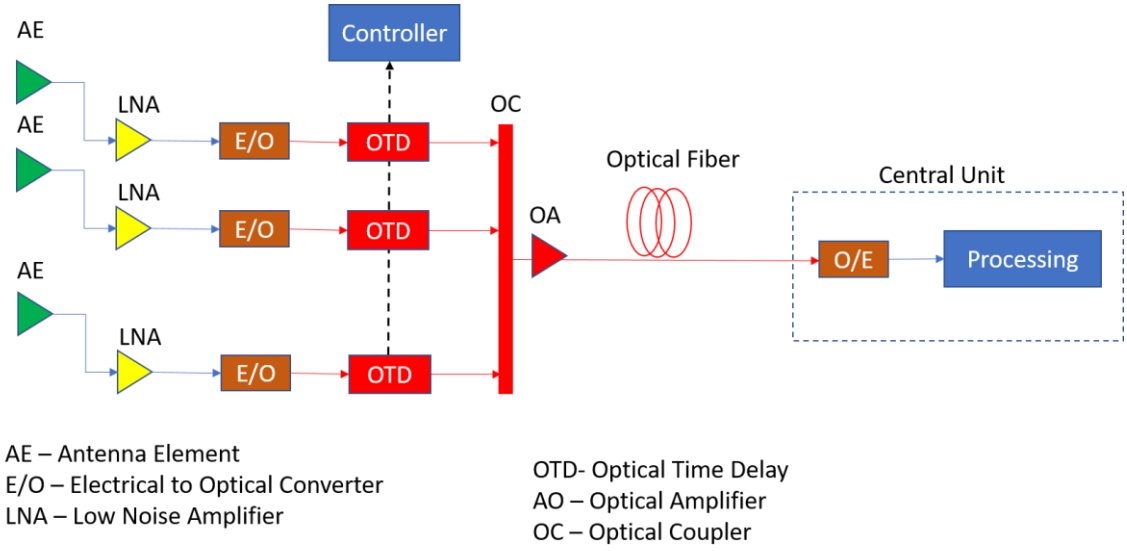

Figure 5. 1 - Block Diagram of Photonic Beam former system Receiver, image adapted from [35] red – optical domain; blue – electrical domain;

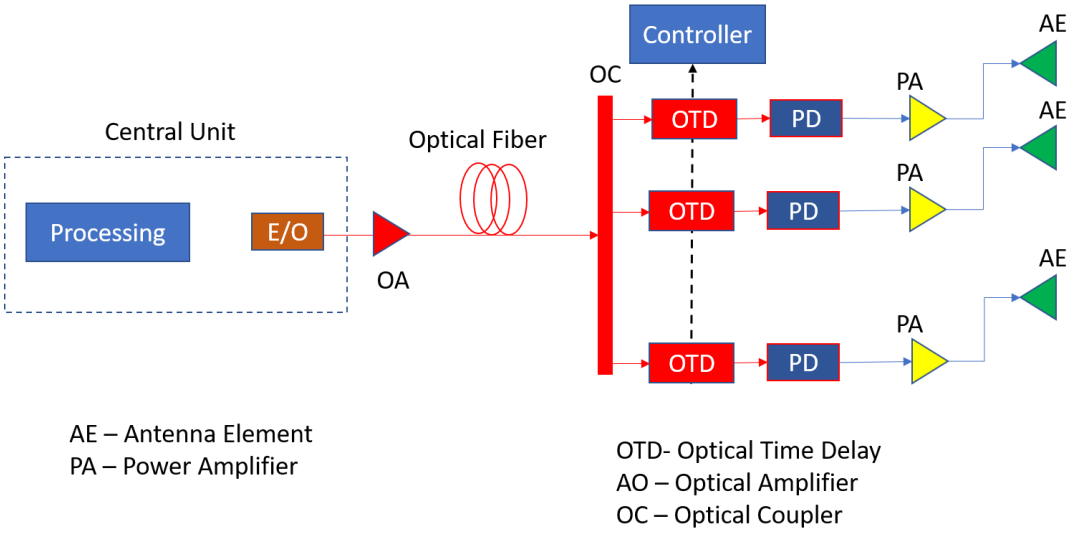

Figure 5. 2 - Block Diagram of Photonic Beam former system Transmitter, image adapted from [35] red – optical domain; blue – electrical domain

5.3 Optical System Model

The system model is depicted in Figure 5. 3. The wireless signal received by the AE is amplified and modulates an optical carrier with frequency v_o, by means of an optical single side band modulator. This approach is based on references [15][20].

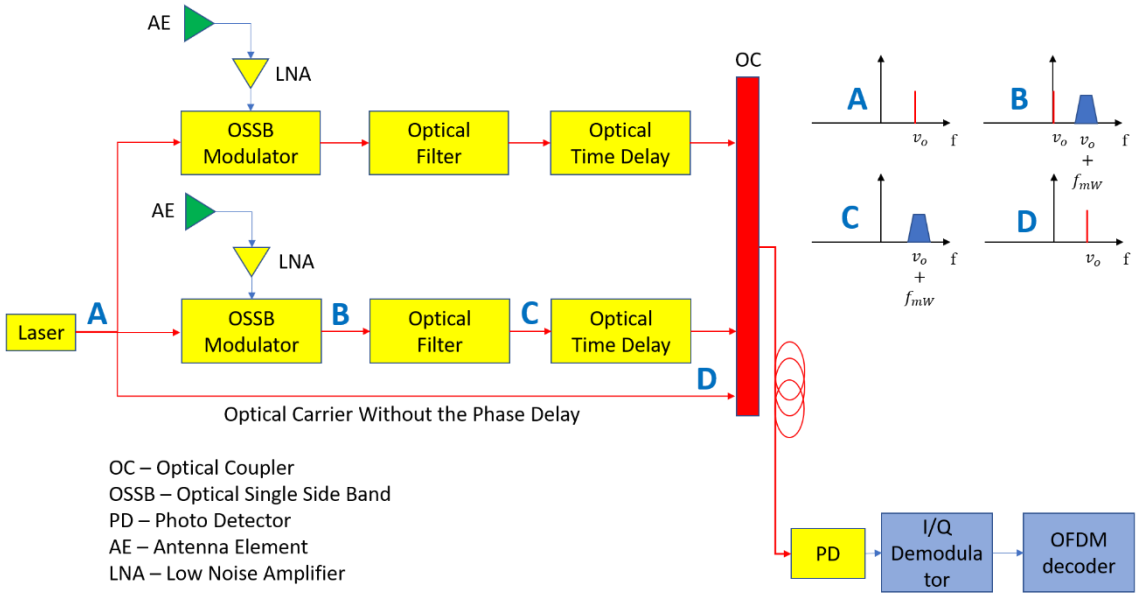

Figure 5. 3 - Reception Block diagram and respective signals

The normalized field of the optical signal at the output of the modulator can be expressed as:

$$E(t) = e^{-i2\pi v_o t} + \tilde{x}_{OFDM}(t)e^{-i2\pi(v_o+f_{RF})t} \tag{5.1}$$

The first term is the optical carrier and the second term is the OFDM baseband signal located at $v_o + f_{RF}$, as illustrated in Figure 5. 3. The next step is to remove the optical carrier, by means of an optical filter and add an optical time delay to the signal band. The introduced optical delay, $n\tau_o$, corresponds to a linear phase shift $\varphi_n(t) = 2\pi n\tau_o t$. After the phase shift the optical signal is combined with an unmodulated optical carrier, resulting in:

$$E_{\varphi_n}(t) = e^{-j2\pi v_o t} + \tilde{x}_{OFDM_n}(t)e^{-j2\pi(v_o+f_{RF})t}e^{-j\varphi_n(t)} \tag{5.2}$$

After, the signal is photo detected by a photodetector with responsivity R. The generated photocurrent, $I_n(t)$ can be calculated as:

$$I_n(t) = R\{E_{\varphi_n}(t).E^*_{\varphi_n}(t)\} \tag{5.3}$$

superscript "$*$" carries out the complex conjugation operation. After some algebraic manipulations and considering $R = 1$ (A/W), it can be shown that $I_n(t)$, can be expressed as:

$$\begin{aligned} I_n(t) = 2 + 2x_{In}cos\big(2\pi f_{RF}t + \varphi_n(t)\big) - 2x_{Qn}sin\big(2\pi f_{RF}t + \varphi_n(t)\big) \\ + \tilde{x}_{OFDM_n}(t)\tilde{x}^*_{OFDM_n}(t) \end{aligned} \tag{5.4}$$

The second and third terms, correspond to the phase shifted components of the baseband OFDM signal. These delayed components can be recovered after the photodetector by an I/Q demodulator.

In a general case, considering *N* antenna elements

$$\begin{aligned} I(t) = 2 + 2\sum_{n=0}^{N-1} x_{In}cos\big(2\pi f_{RF}t + \varphi_n(t)\big) \\ - 2\sum_{n=0}^{N-1} x_{Qn}sin\big(2\pi f_{RF}t + \varphi_n(t)\big) \\ + \sum_{n=0}^{N-1} \tilde{x}_{OFDM_n}(t)\tilde{x}^*_{OFDM_n}(t) \end{aligned} \tag{5.5}$$

5.4 Optical Time Delay and Optical Phase Shifter Implementations

The first proposed optical delays were based on bulky switchable delay matrices, in which discrete delays are implemented with fibers of different lengths [16]. More compact and continuously tunable photonic beamforming systems based on dispersive devices were also proposed in [26], in which the delay given to a signal depends on its wavelength and/or on the center wavelength of the dispersive device. Photonic integration technique is promising to significantly reduce the hardware volume. In [27], a remotely tuneable integrated optical TTD based on an arrayed waveguide grating feedback loop (AWG-loop) is presented. Since the AWG is used as both the wavelength multiplexer and the de-multiplexer, the AWG-loop allows a compact, fabrication tolerant and scalable solution for feeding more antenna elements. Recently, the same design was tested in the 38 GHz band links with bit rates from 50 Mb/s to 8 Gb/s per spatial channel [27]. An approach that relies on simple tuneable optical delay lines and also on self-heterodyne coherent detection was also demonstrated in [14]. An ultrafast beam steering scheme was demonstrated in [28] for multi target detection. Although photonic integration technique has shown promising results, transmission and steering performance needs to be improved such as the scanning angle, throughput, and driver electronics/packaging.

Tunable optical delay lines bring many advantages such as cost reduction, the small size and easy integration with modulation or filtering. All those optimal characteristics gave origin to many works and studies around the implementation of a true-time delay line that can control the delay of a given optical signal. There are two main classes of implementation, the first class has the devices that take advantage of resonant enhancement, the second class has the delay lines structures that don't take advantage of resonant enhancement. In the first class of devices the incident light power is controlled using an optical cavity (linear cavity o ring resonator), if the cavity is mode-matched and resonant with the incident light, the power inside the cavity is going to be higher than the incident power, using this principle tunable delays can be achieved making the light recirculate creating a group delay. In the second class the amount of delay is directly dependent with the size of the device because it's made with actual lines of different lengths.

One of the most popular delay lines are the ring resonators, they belong to the first class of true time delay devices. Comparing it with the non-resonant techniques for delay lines we see that with the ring resonator we can achieve longer delays at the cost of a smaller bandwidth, big losses and a complex tuning of the delay. With non-resonant delay lines we will achieve shorter delays but with higher bandwidth compatibility, much lower losses and more control over the delay [21], in the case of the MZ based true time delay we can control the delay continuously using only one signal.

5.5 Photonic Supported Beam Steering Based on Continuously Tuneable Mach-Zehnder Interferometer (CT_MZI)

5.5.1 CT-MZI Structure

The CT-MZI considered was proposed in [21] and it was the system selected for this dissertation. This component provides delay that can be dynamically and continuously adjusted. It consists of a Mach-Zehnder (MZ) interferometer with two tunable couplers.

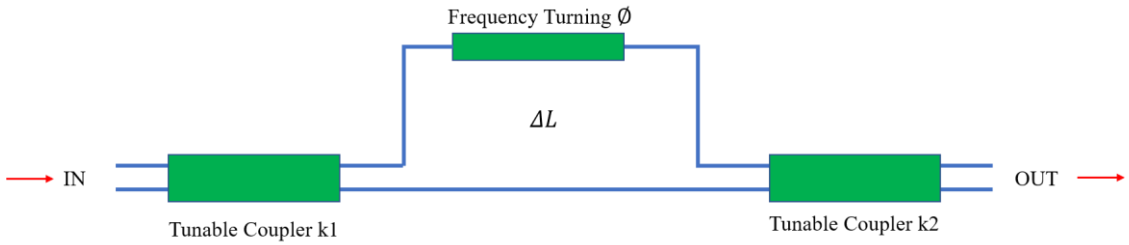

Figure 5. 4 - CT-MZI Structure, figure adapted from [18]

A MZ interferometer is an optical device constituted by two inputs, two paths, two beam splitters and two outputs. The beam splitters rearrange half of the two input beams to both the output channels and the two mirrors that reflect the beam [29] [30] [31] as we can see in the Figure 5. 5.

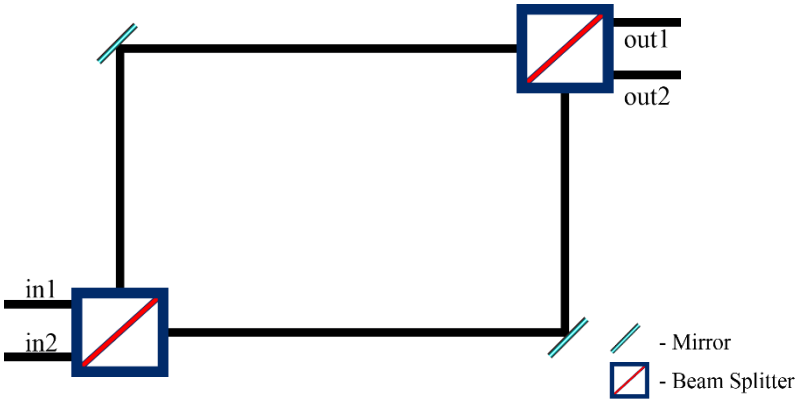

Figure 5. 5 - Mach-Zehnder interferometer

5.5.2 Mathematical Model of CT-MZI

Considering a different length for each path (ΔL), and with a constant phase shift applied through the phase shifter integrated in the interferometer , the transfer function of the MZ interferometer [32] can be written as:

$$\begin{bmatrix} E_{out_1} \\ E_{out_2} \end{bmatrix} = \begin{bmatrix} e^{-j\emptyset_1} & 0 \\ 0 & e^{-j\emptyset_2} \end{bmatrix} \begin{bmatrix} E_{in_1} \\ E_{in_2} \end{bmatrix} \tag{5.6}$$

$$\emptyset_i = 2\pi f \tau_i + \emptyset \tag{5.7}$$

Where f is the frequency, τ_i is the time delay introduced by path *i* and $\emptyset$ a constant phase shift. The time unbalance between the two arms of the interferometer, T, is defined as:

$$T = \frac{n_g \Delta L}{c} = \frac{1}{FSR} \tag{5.8}$$

ΔL, is the length difference between the two paths, c, velocity of light, n_g, the material group index and FSR is the Free Spectral Range.

To achieve the linear control over the delay two tuneable couplers replace the beam splitters. The coupling ratio of the couplers, k_1 and k_2, varies from 0 to 1. To achieve a continuous control over the delay and to simplify the complexity of the system both couplers will have the same coupling ratio, $k_1 = k_2 = k$, in this way we can control both using a single signal.

The transfer function of the coupler is as follows:

$$\begin{bmatrix} E_{out_{coupler_1}} \\ E_{out_{coupler_2}} \end{bmatrix} = \begin{bmatrix} \sqrt{1-k} & j\sqrt{k} \\ j\sqrt{k} & \sqrt{1-k} \end{bmatrix} \begin{bmatrix} E_{in_{coupler_1}} \\ E_{in_{coupler_2}} \end{bmatrix} \tag{5.9}$$

The transfer function of the complete system [33] can be written as:

$$\begin{bmatrix} E_{out_1} \\ E_{out_2} \end{bmatrix} = \begin{bmatrix} \sqrt{1-k} & j\sqrt{k} \\ j\sqrt{k} & \sqrt{1-k} \end{bmatrix} \begin{bmatrix} \mathrm{e}^{-\mathrm{j}\emptyset_1} & 0 \\ 0 & \mathrm{e}^{-\mathrm{j}\emptyset_2} \end{bmatrix} \begin{bmatrix} \sqrt{1-k} & j\sqrt{k} \\ j\sqrt{k} & \sqrt{1-k} \end{bmatrix} \begin{bmatrix} E_{in_1} \\ E_{in_2} \end{bmatrix} \tag{5.10}$$

Considering only input 2 and output 2, therefore:

$$E_{out_2} = \left(-k\mathrm{e}^{-\mathrm{j}\emptyset_1} + (1-k)\mathrm{e}^{-\mathrm{j}\emptyset_2}\right) E_{in2} \tag{5.11}$$

$$\emptyset_0 = \frac{(\emptyset_1 + \emptyset_2)}{2} \tag{5.12}$$

$$\Delta\emptyset = \emptyset_1 - \emptyset_2 \tag{5.13}$$

We can simplify this function using equations (5.12) and (5.13) resulting a simpler function that only depends on the difference of phase between paths $\Delta\emptyset$, this way the transfer function H comes as follows:

$$\frac{E_{out_2}}{E_{in_2}} = H = e^{-j\emptyset_2}(-k\mathrm{e}^{-\mathrm{j}\Delta\emptyset} + 1 - k) \tag{5.14}$$

Considering the smallest path negligible, $\emptyset_2 \approx 0$ and the relation between frequency and phase shown in equation (5.15), we achieve the final form of the transfer function as shown in equation (5.16):

$$\Delta\emptyset = 2\pi\,\mathrm{f}\,\Delta\mathrm{t} + \Phi,\ \Delta\mathrm{t} = \frac{\Delta\mathrm{L}}{\mathrm{c}} n_g \tag{5.15}$$

$$H(f,k) = -k\mathrm{e}^{-\mathrm{j}2\pi\,\mathrm{f}\,\Delta\mathrm{t}+\Phi} + 1 - k \tag{5.16}$$

Having the transfer function, we can obtain de Power transfer function from $|H(f,k)|^2$ and the group delay as function of the frequency from $\frac{d(\angle H(f,k))}{d\theta}$:

$$\angle H(f,k) = \mathrm{atan}\left(\frac{k\,sin(\Delta\emptyset)}{1-k-k\,cos(\Delta\emptyset)}\right) \tag{5.17}$$

Figure 5. 6 show the power transmission and the normalized group delay versus the operating optical frequency normalized to FSR, for different values of k.

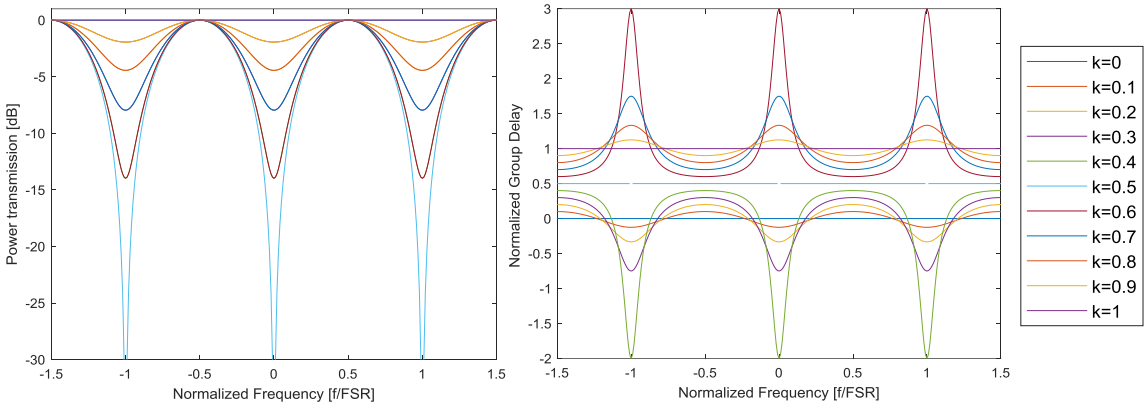

Figure 5. 6 -Power Transmission (left) Normalized Group Delay (right)

As we can see in Figure 5. 6 the effective bandwidth is approximately $\frac{FSR}{2}$ and the delay in it is not always linear, this will introduce a small amount of squint to the system.

Figure 5. 7 shows the normalized group delay as function of the coupling parameter for the frequency $\frac{f}{FSR} = 0.5$ and $\frac{f}{FSR} = 0.25$. We note that while the normalized group delay increases linearly with k for $\frac{f}{FSR} = 0.5$, the same does not apply for the other

frequencies. This means that the CT-MZI operates an ideal optical time delay only when k=0.5.

5.6 Design Guidelines

We identify four design requirements:

a) the maximum steering angle, θ_{max};

b) the number of antenna elements, N;

c) the mmWave operating range, f_{mW};

d) the wireless signal bandwidth, B_{OFDM}

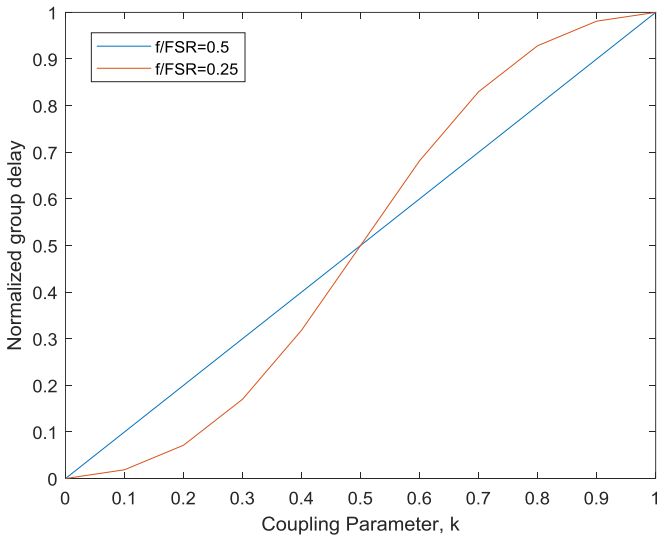

Figure 5. 7 - Relation between the control signal and the normalized delay

5.6.1 Maximum Delay Requirements

Requirements a), b) and c) set the maximum delay that is necessary to compensate owing to the beam squint. Considering the distance between AEs, $d = \frac{\lambda}{2}$, from equation (3.3), the maximum delay, $\tau_{max,AE}$, that needs to be compensated at the output of the antenna element N is:

$$\tau_{max,AE} = \frac{(N-1)}{2f_{mW}} sin(\theta_{max}) \tag{5.18}$$

On the other hand the maximum delay provided by the CT-MZI structure is given by equation (5.20)

$$\tau_{max,MZI} = \frac{n_g \Delta L}{c} \tag{5.19}$$

From equations (5.19) and (5.20), the required length difference of the two arm of the MZI, ΔL, can be calculated.

$$\Delta L = \frac{(N-1)c}{2 f_{mW} n_g} sin(\theta_{max}) \tag{5.20}$$

ΔL, will set the size of the chip. Small chip sizes are required not only because it is desirable to have component with small dimensions but also because the propagation losses in the waveguide, which are of the order of 2 dB/cm [34], can lead to unsupportable power losses for large path lengths. In order to reduce ΔL, it is necessary materials with high n_g, additionally operation at high mmWaves will also lead to chips with reduced size.

Figure 5. 8 shows the required ΔL versus the maximum steering angle for number of PAA antenna elements, N. Operation at $f_{mW} = 20\ GHz$ and $n_g = 3.51$ [34] were

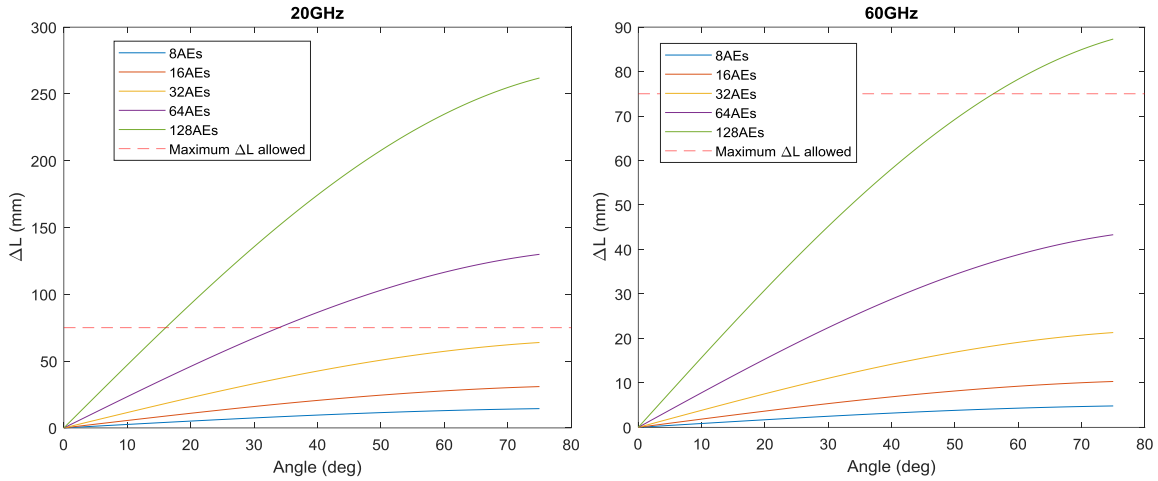

Figure 5. 8 - Relation Between length and maximum steering angle for 20GHz (left) and for 60GHz (right) without digital squint compensation

considered. Assuming, that the attenuation loss limit for the ΔL is 15 dB, the maximum is $\Delta L = 75\ mm$. This value will set the operational limit of this implementation. For example, if $N = 128$, the maximum achievable steering angle with squint compensation is $\theta_{max} = 20º$. If a higher maximum steering angle is required, the number of antenna elements have to be reduced.

Figure 5. 8 shows that when $f_{mW} = 60\ GHz$ the system allows operation with larger steering angles with larger number of AEs when compared with $f_{mW} = 20\ GHz$.

5.6.2 Signal Bandwidth Requirements

We note from the power transfer function of the CT-MZI Figure 5. 6, that the bandwidth of the device is limited. The minimum 3-dB bandwidth around a power transmission

maximum occurs when k=0.5 and is $B_{3dB,max} = \frac{FSR}{2}$, this bandwidth limitation will set the limit value for FSR. We also note that the group delay introduced by the CT-MZI is not constant within the bandwidth, therefore different frequency components will experience different propagation delays, leading to signal dispersion in the time domain. To avoid the bandwidth limitation, the FSR of the device should be set as large as possible. However, according to equation 5.8 the maximum delay that is introduced by the CT-MZI is inversely proportional to FSR.

As design criteria we will use the following equation:

$$B_{OFDM,wireless} = \frac{FSR}{2} \tag{5.21}$$

where $B_{OFDM,wireless}$, is the bandwidth of the wireless signal.

Figure 5. 9 shows the localization of the wireless signal in the optical domain within the power transmission transfer function of the CT-MZI. In order to achieve the maximum power transmission, the spectrum of wireless signal in the optical domain should be located at a maximum of the CT-MZI power transfer function, which can be expressed as,

$$f_{mW} = (i - 0.5)FSR, \text{ where } i \text{ is an integer and } i \geq 1. \tag{5.22}$$

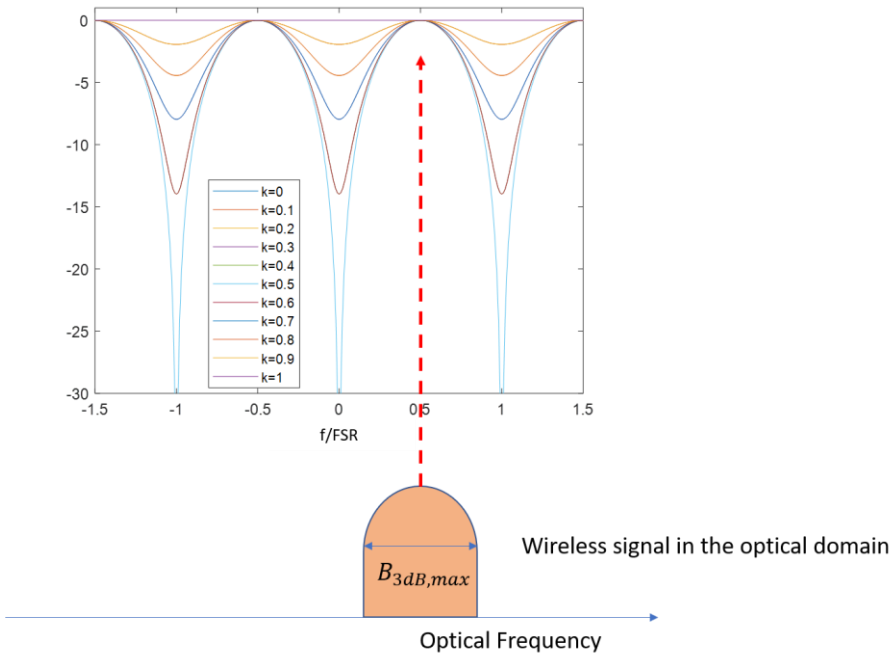

Figure 5. 9 - Demonstration of the bandwidth available for the wireless signal in the optical domain

By its turn, from equation (5.8), we note that FSR is inversely proportional to ΔL, therefore to increase the usefull bandwidth we need to increase FSR which can be achieved by decreasing ΔL, as shown in Figure 5. 10, which depicts the wireless signal bandwidth versus the required ΔL, for $f_{mW} = 20\ GHz$ and $f_{mW} = 60\ GHz$.

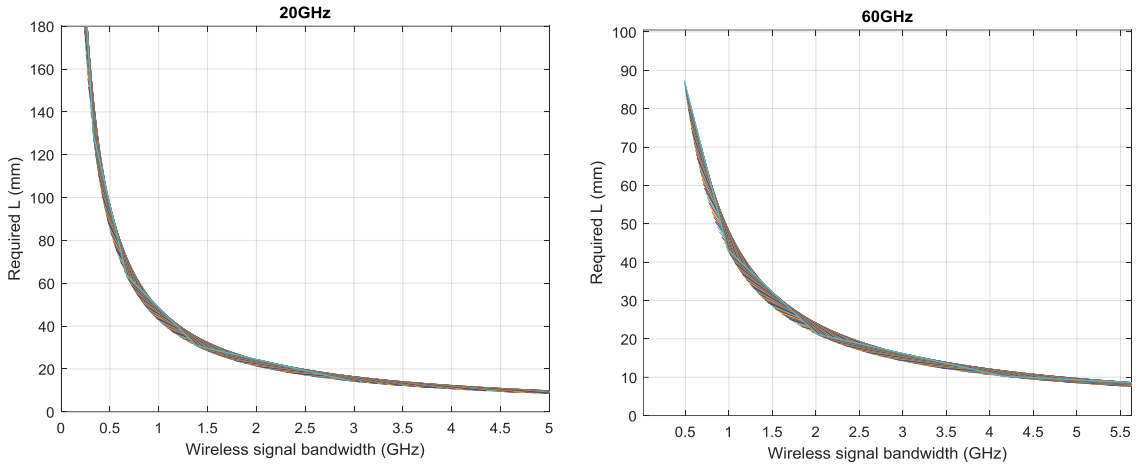

Figure 5. 10 - Relation between the wireless signal bandwidth and the requires length for 20GHz(left) and 60GHz (right)

A conservative design guideline is: calculate $\Delta L'$ according the bandwidth requirements and calculate $\Delta L''$ according to the beam squint compensation requirements and choose the minimum for the chip design.

5.7 Dimensioning Example

We consider that all CT-MZIs at each antenna element are identical, i.e ΔL is constant for all CT_MZIs. The OFDM parameters are the ones that were considered in section 4.5.

1) Calculate $FSR = 2B_{OFDM,mW} = 1.25\ GHz$.
2) Re-calculate FSR to obey equation (5.23). $FSR = \frac{20e9}{(15+0.5)} \approx 1.29\ GHz$
3) Calculate the required device $\Delta L = 66.6\ mm$

According to Figure 5. 8 (left) with AEs=32 the squint effect should be compensated, however this was not observed, the EVM values obtained, for steering angles different from 0, where well above the EVM limit value. The next step was to verify if the system performance could be improved by increasing the FSR value of the device. Aceptable EVM values were achieved by increasing the FSR up to 3.08 GHz, 3.64 GHz and 4.44 GHz as can be observed in Figure 5. 11. It interesting to note in Figure 5. 11 that the system presents very high EVM values for small steering angles. This behaviour, not aceptable for a practical implementation, can be explained by the CT-MZI dimensioning. All the CT-MZI for the different AEs have the same length, and for small

steering angles, the k parameter is set to a very small value. According to Figure 5. 7, for small values of k, the delay added by the CT-MZI is not constant to all frequency components, which lead signal dispersion and increased EVM.

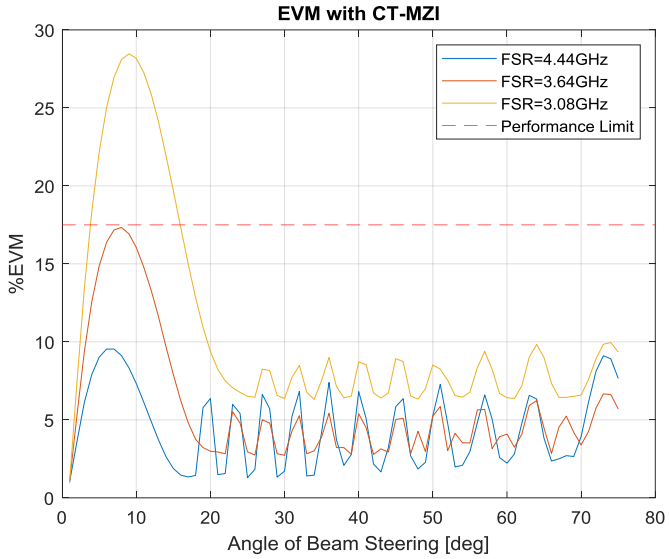

Figure 5. 11 - EVM of the system varying with FSR without digital compensation

Considering FSR=3.64 GHz, this corresponds to a device with $\Delta L = 23.5\, mm$, which is not enough to add the necessary total compensation delay to all AEs. However, the overall achieved performance is acceptable. The performance of the system can still be improved if digital beam squint compensation is applied as illustrated in Figure 5. 12.

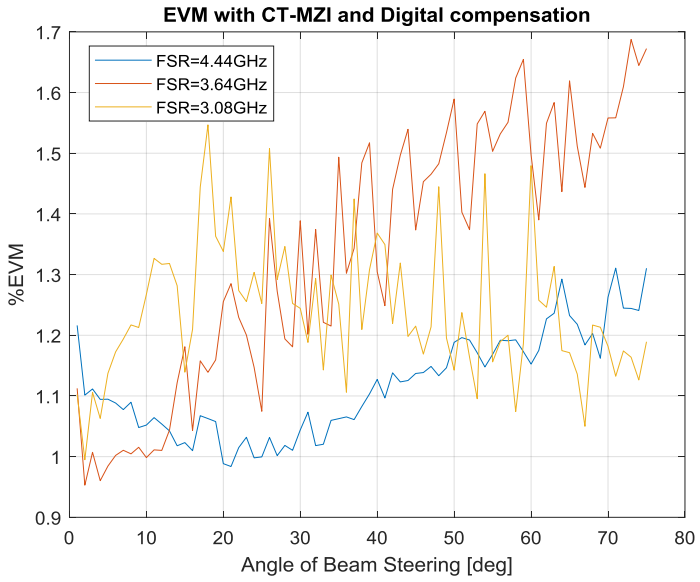

Figure 5. 12 - EVM of the system varying with FSR with digital squint compensation.

5.8 Comment on the Suitability of CT-MZI Structure for Beam Steering

CT-MZI structures provide a means to continuously steer an mmWave beam, by controlling the value of the coupling parameter k. However, due to the compromise of bandwidth against delay, their application is limited. Our simulation results pointed out the need to optimize the length of the device to be used for specific antenna element.

6 Conclusion and Future Work

Phased Array Antennas (PAAs) controlled by optical steering devices is a very promising area, particularly due to the recent advances on microwave photonic integrated circuits. Photonic integration is particularly advantageous since allow to reduce costs and sizes of the devices and enable integration with other functional circuits. Another important aspect of photonics solutions is the ability to comply novel 5G network architectures that are supported by the use of optical fiber transmission in the fronthaul network segment used to deliver and receive the wireless signals from the antennas.

Beam steering based on optical technology is a timely relevant topic, with a huge variety of proposals been published. In this context it is of key importance to have a tool to assess the effect of these schemes on the system performance as well as to provide feedback to be used in the optimization of the devices and subsystems.

In this dissertation, we have implemented a simulation tool, in Matlab that enables the study and performance evaluation of photonic based steering techniques. The simulation model is very simple, and in the future, it needs to be improved including other functionals blocks such as: the wireless channel model, the noise added by the electrical and optical components as well as aspects of fiber transmission.

The developed simulation evaluated the effects of PAA using electric phase shifter to have a comparison point with the new optical steering devices. The Beam squint was evident. Performance numbers were saved for different systems. Digital compensation was also tested, and the results save for a later comparison.

Using our simulation model, we have demonstrated that:

The actual simulation has several approximations and considerations such as perfect wireless channel, no noise from the electric components and distortions from fiber transmissions. Future work can be to include those options in the simulation to achieve more realist results.

Digital baseband compensation of the beam squint effect is very efficient, however, our results have shown that in some situations it is not enough to compensate the beam squint effect. Future work can be to identify why this happens.

Initially the dimensioning of the CT-MZI was made with a compromise between FSR and the maximum delay. After the simulation we conclude that the FSR is a more important parameter. In future work the dimensioning of the CT-MZI will take that into account.

Using a CT-MZI for photonic beam steering it was evident that the system needs improvements. The different AEs cannot have the same CT-MZI. The use of smaller coupling factors introduces higher distortions. Future work will be to project individual CT-MZI for the different AEs of the PAA.

7 References

[1] D. Webster, “Cisco Visual Networking Index: Global Mobile Data Traffic Forecast Update, 2016–2021,” *Global Forecast Update*, 2017. [Online]. Available: https://www.cisco.com/c/en/us/solutions/service-provider/visual-networking-index-vni/white-paper-listing.html.

[2] Q. Technologies, “Spectrum for 4G and 5G Licensed spectrum spectrum spectrum,” 2017. [Online]. Available: https://www.qualcomm.com/media/documents/files/spectrum-for-4g-and-5g.pdf. [Accessed: 01-Nov-2018].

[3] K. Sakaguchi *et al.*, “Where , When , and How mmWave is Used in 5G and Beyond,” 2018. [Online]. Available: https://arxiv.org/ftp/arxiv/papers/1704/1704.08131.pdf. [Accessed: 01-Nov-2018].

[4] I. Public and P. Partnership, “The 5G Infrastructure Public Private Partnership: the next generation of communication networks and services.” [Online]. Available: https://5g-ppp.eu/wp-content/uploads/2015/02/5G-Vision-Brochure-v1.pdf. [Accessed: 01-Nov-2018].

[5] L. A. N. Man, S. Committee, and I. Computer, *Part 11 : Wireless LAN Medium Access Control (MAC) and Physical Layer (PHY) Specifications Amendment 3 : Enhancements for Very High Throughput in the 60 GHz Band IEEE Computer Society*, vol. 2012, no. December. 2012.

[6] S. Rangan, T. S. Rappaport, and E. Erkip, “Millimeter-Wave Cellular Wireless Networks : Potentials and Challenges,” *Proc. IEEE*, vol. 102, no. 3, pp. 366–385, 2014.

[7] C. A. Balanis, *Antenna Theory: Analysis and Design*, 3rd ed., vol. 28, no. 3. Wiley-Interscience, 2012.

[8] Z. Pi and F. Khan, “System design and network architecture for a millimeter-wave mobile broadband (MMB) system,” *2011 34th IEEE Sarnoff Symp. SARNOFF 2011*, 2011.

[9] W. Roh *et al.*, “Millimeter-Wave Beamforming as an Enabling Technology for 5G Cellular Communications : Theoretical Feasibility and Prototype Results,” *IEEE Commun. Mag.*, vol. 52, no. February, pp. 106–113, 2014.

[10] S. Kutty and D. Sen, “Beamforming for Millimeter Wave Communications: An Inclusive Survey,” *IEEE Commun. Surv. Tutorials*, vol. 18, no. 2, pp. 949–973, 2016.

[11] D. G. Fang, “Arrays and Array Synthesis,” in *Antenna theory and microstrip antennas*, vol. 136, no. 1, Taylor & Francis Group, 2010, pp. 33–84.

[12] Kraus, “Antennas.” .

[13] F. Ellinger *et al.*, “Integrated adjustable phase shifters,” *IEEE Microw. Mag.*, vol. 11, no. 6, pp. 97–108, 2010.

[14] X. S. Yao, “A Tutorial on Microwave Photonics Including : True-time Delay Beamforming,” vol. 26, no. 3, IEEE photonics society news, Ottawa, Ontario, 2012.

[15] V. C. Duarte, M. V. Drummond, and R. N. Nogueira, “Photonic True-Time-Delay Beamformer for a Phased Array Antenna Receiver based on Self-Heterodyne Detection,” *J. Light. Technol.*, vol. 34, no. 23, pp. 5566–5575, 2016.

[16] I. Frigyes, S. Member, A. J. Seeds, and S. Member, “Optically Generated True-Time Delay in Phased-Array Antennas,” *IEEE Trans. Microw. Theory Tech.*, vol. 43, no. 9, 1995.

[17] L. Wille Ng and A. A. Walston, “The First Demonstration Of An Optically Steered Microwave Phased Array Antenna Using True-Time-Delay,” *J. Light. Technol.*, vol. 9, no. 9, pp. 1124–1131, 1991.

[18] Z. Cao *et al.*, “Cyclic Additional Optical True Time Delay for Microwave Beam Steering with Spectral Filtering,” *Opt. Lett.*, vol. 39, no. 12, pp. 3402–3405, 2014.

[19] P. D. Lines, “Photonic Integrated Circuits for Tunable Delay Lines.”

[20] G. Serafino *et al.*, “Photonics-assisted beamforming for 5G communications,” *IEEE Photonics Technol. Lett.*, vol. 30, no. 21, pp. 1826–1829, 2018.

[21] D. Melati, A. Waqas, Z. Mushtaq, and A. Melloni, “Wideband Integrated Optical Delay Line Based on a Continuously Tunable Mach – Zehnder Interferometer,” *IEEE J. Sel. Top. Quantum Electron.*, vol. 24, no. 1, pp. 1–8, 2018.

[22] Google Project, “Stadia,” 2019. [Online]. Available: https://stadia.dev/about/. [Accessed: 07-Jun-2019].

[23] Nvidea, “Geforce Now.” [Online]. Available: https://www.nvidia.com/en-us/geforce/products/geforce-now/. [Accessed: 07-Jun-2019].

[24] M. Cai, “Modeling and Mitigating Beam Squint in Millimeter Wave Wireless Communication,” University of Notre Dame, 2018.

[25] G. Debatosh and M. M. A. Yahia, *Microstrip and Printed Antennas: New Trends, Techniques and Applications*, 1st ed. Wiley.

[26] I. Uchendu and J. R. Kelly, “Survey of Beam Steering Techniques Available for Millimeter Wave Applications,” *Prog. Electromagn. Res. B*, vol. 68, no. January 2016, pp. 35–54, 2016.

[27] R. A. Shafik, M. S. Rahman, and A. H. M. R. Islam, “On the extended relationships among EVM, BER and SNR as performance metrics,” *Proc. 4th Int. Conf. Electr. Comput. Eng. ICECE 2006*, no. December, pp. 408–411, 2007.

[28] Rohde & Schwarz, O. Werther, and R. Minihold, “LTE System Specifications and their Impact on RF & Base Band Circuits,” *Rohde Schwarz App Note*, p. 37, 2013.

[29] Max Born and Emil Wolf, “Principles of optics,” p. 936, 2003.

[30] J. G. Rarity *et al.*, “Two-photon interference in a Mach-Zehnder interferometer,” *Phys. Rev. Lett.*, vol. 65, no. 11, pp. 1348–1351, 1990.

[31] L. Vaidman, “Interaction-Free Measurements,” pp. 1–7, 1994.

[32] M. C. S. Blanco and T. Engineering, “Spectral Amplitude and Phase Characterization of Optical Devices by RF scan.”

[33] R. H. M. O’Sullivan, *Fiber Optic Measurement Techniques*. 2001.

[34] R. Bonjour *et al.*, “Ultra-fast millimeter wave beam steering,” *IEEE J. Quantum Electron.*, vol. 52, no. 1, pp. 1–8, 2016.

[35] J. Stewart, *Calculus Early Trancendentals*. .

8 Appendices

a) 3D Extension

In this work we have been talking about linear arrays that allow us to control the direction of the beam in one dimension. In real world scenarios, if we want to cover a wide area efficiently, we need to be able to steer the beam in two dimensions, that way we can find the user even if he goes near the antenna or up a mountain. To achieve the two-dimension beam steering we need to implement a planar array.

The linear array enables us to control the θ dimension, for example, if the antennas are pointing to the horizon we will be able to steer the beam left and right (θ), but not up and down ($\emptyset$).

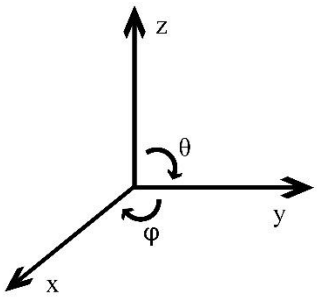

A planar array is a group of linear arrays, let's analyse an example of an 8x8 array, the array factor will now have two variables, ψ_x and ψ_y:

$$\psi_x = \beta d_x sin(\theta)\cos(\phi) + \delta_x$$

$$\psi_y = \beta d_y sin(\theta) sin(\phi) + \delta_y$$

$$\delta_x = -k d_x \sin(\theta_0)\cos(\phi_0)$$

$$\delta_y = -k d_y \sin(\theta_0)\sin(\phi_0)$$

Using the same logic as the linear array, the planar array factor of a MxN planar array comes as follows [11]:

$$\frac{1}{M}\frac{\sin\left(\frac{M}{2}\psi_x\right)}{\sin\left(\frac{\psi_x}{2}\right)}\frac{1}{N}\frac{\sin\left(\frac{N}{2}\psi_y\right)}{\sin\left(\frac{\psi_y}{2}\right)}$$

A simulation of the radiation pattern of the array was implemented in Matlab to better understand its characteristics and capabilities. However, in this work, to reduce the complexity of the simulations, in the system implementation we are only going to use linear arrays. If the theory works in linear arrays it will work on planar arrays as well. In the figure bellow, we can see the radiation pattern of a $8x8$ planar array of microstrip antennas spaced in both directions $\frac{\lambda}{2}$.

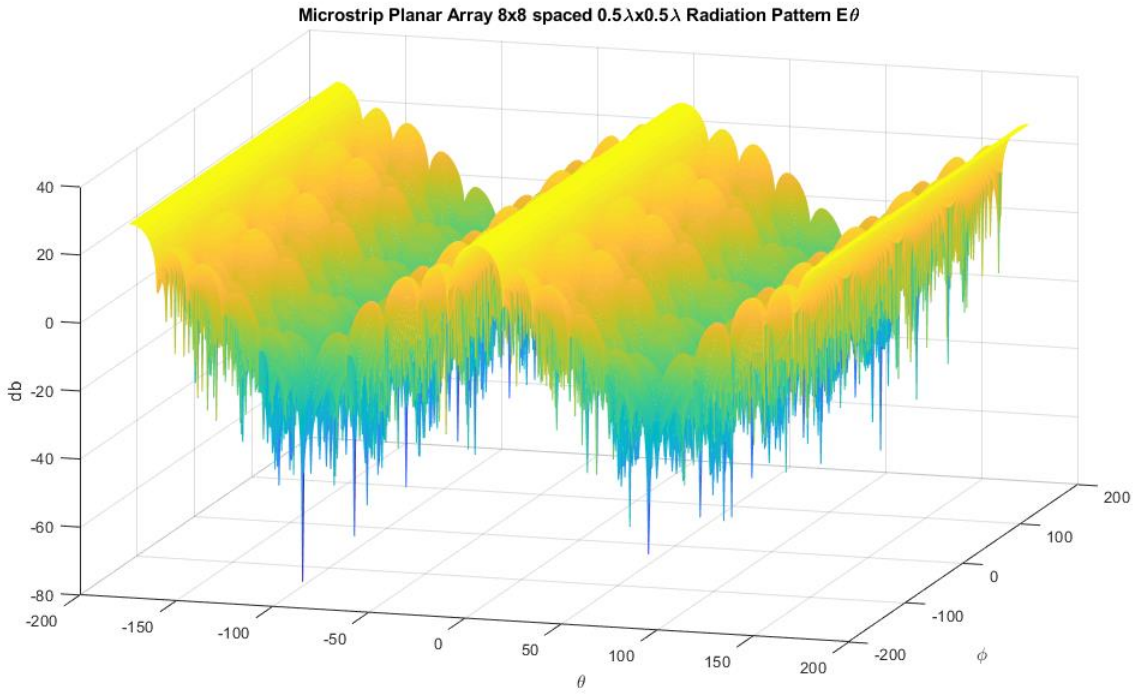
Microstrip Planar Array 8x8 spaced 0.5λx0.5λ Radiation Pattern Eθ
db
40
20
0
-20
-40
-60
-80
-200
-150
-100
-50
0
50
100
150
200
θ
200
100
0
-100
-200
ϕ

b) Mathematical Deduction of the Group Delay

From $\angle H = \text{atan}\left(\frac{-k\,sin(\Delta\emptyset)}{1-k-k\,cos(\Delta\emptyset)}\right)$, to achieve the normalized group delay (τ_N) equation we used the following mathematical relations [35]:

$$\left(\frac{u}{v}\right)' = \frac{(u'v - uv')}{v^2}$$

$$f\big(g(x)\big)' = f'\big(g(x)\big)g'(x)$$

$$\tau_{Norm} = \frac{d(\angle H)}{d\theta} = \frac{k\big(k - \cos(\Delta\emptyset) + kcos(\Delta\emptyset)\big)}{2k^2\cos(\Delta\emptyset) - 2kcos(\Delta\emptyset) - 2k + 2k^2 + 1}$$

c) Example of a PAA Array Factor For Two Elements

With the creation of the following variable (ψ) and some manipulation, we can present a more visually appealing formulation to obtain the array factor of the PAA. For instance, the formulation for two elements with the same radiation pattern E_0 and considering the reference for the phase the centre of the array is as follows:

$$E_{total} = E_0 e^{-\frac{j\psi}{2}} + E_0 e^{\frac{j\psi}{2}} \tag{3.21}$$

$$\psi = \beta d cos(\theta) + \delta \tag{3.22}$$

β is the propagation constant and δ is the phase shift from each antenna element. In ψ variable, the $\beta d cos(\theta)$ corresponds to the difference distances between each element and the user just like $(a(\theta, f))$. δ corresponds to the phase shift compensation shown in equation (3.6). After some manipulation using Euler's formula we obtain array factor equation (3.10) equal to [7] and [11]:

$$\frac{\sin(\psi)}{\sin\left(\frac{\psi}{2}\right)} \equiv \frac{\sin\left(\frac{N\psi}{2}\right)}{\sin\left(\frac{\psi}{2}\right)}, N = 2 \tag{3.23}$$

The array factor allows us to simulate the effect of an array in the radiation pattern. By using the Theory of Aggregates that states that the resulting radiation pattern of an antennas array is the radiation of a single element multiplied by the array factor. Using this method, it may be easier and simpler to understand and obtain the radiation pattern.